(2)

STUDY OF THE INFLUENCE OF METALLURGICAL FACTORS ON FATIGUE AND FRACTURE OF AEROSPACE STRUCTURAL MATERIALS

by
James Lankford
David L. Davidson
Gerald R. Leverant
Kwai S. Chan

AFOSR ANNUAL REPORT

This research was sponsored by the Air Force Office of Scientific Research,
Electronic and Materials Sciences Directorate
Under Contract F49620-83-C-0054

Approved for release; distribution unlimited.

February 1985

SOUTHWEST RESEARCH INSTITUTE
SAN ANTONIO HOUSTON

AFOSR-TR- 85-0372

SOUTHWEST RESEARCH INSTITUTE
Post Office Drawer 28510, 6220 Culebra Road
San Antonio, Texas 78284

STUDY OF THE INFLUENCE OF METALLURGICAL FACTORS ON FATIGUE AND FRACTURE OF AEROSPACE STRUCTURAL MATERIALS

by
James Lankford
David L. Davidson
Gerald R. Leverant
Kwai S. Chan

AFOSR ANNUAL REPORT

This research was sponsored by the Air Force Office of Scientific Research,
Electronic and Materials Sciences Directorate
Under Contract F49620-83-C-0054

Approved for release; distribution unlimited.

February 1985

Approved:

U. S. Lindholm, Director
Department of Materials Sciences

UNCLASSIFIED

SECURITY CLASSIFICATION OF THIS PAGE (When Data Entered)

REPORT DOCUMENTATION PAGE	READ INSTRUCTIONS BEFORE COMPLETING FORM
1. REPORT NUMBER: AFOSR-TR- 85-0372	2. GOVT ACCESSION NO.: AD A153913
	3. RECIPIENT'S CATALOG NUMBER:
4. TITLE (and Subtitle): Study of the Influence of Metallurgical Factors on Fatigue and Fracture of Aerospace Structural Materials	5. TYPE OF REPORT & PERIOD COVERED: Annual Scientific Report 1 Jan 1984 - 31 Dec 1984
	6. PERFORMING ORG. REPORT NUMBER: 06-7436
7. AUTHOR(s): James Lankford, David L. Davidson, Gerald R. Leverant, Kwai S. Chan	8. CONTRACT OR GRANT NUMBER(s): F49620-83-C-0054
9. PERFORMING ORGANIZATION NAME AND ADDRESS: Southwest Research Institute, 6220 Culebra Road (P.O. Drawer 28510), San Antonio, TX 78284	10. PROGRAM ELEMENT, PROJECT, TASK AREA & WORK UNIT NUMBERS: 61102F, 2306, A1
11. CONTROLLING OFFICE NAME AND ADDRESS: AF Office of Scientific Research, Bolling AFB, Building 410, Washington, DC 20332	12. REPORT DATE: February 1985
	13. NUMBER OF PAGES: 39
14. MONITORING AGENCY NAME & ADDRESS (if different from Controlling Office)	15. SECURITY CLASS. (of this report): UNCLASSIFIED
	15a. DECLASSIFICATION/DOWNGRADING SCHEDULE

16. DISTRIBUTION STATEMENT (of this Report)

Approved for public release; distribution unlimited.

17. DISTRIBUTION STATEMENT (of the abstract entered in Block 20, if different from Report)

18. SUPPLEMENTARY NOTES

19. KEY WORDS (Continue on reverse side if necessary and identify by block number)

Fatigue	Titanium Alloys
Fracture	Single Crystals
Crack Growth	Crack Tip Plasticity
Nickel-Base Superalloys	Crack Growth Modeling
Aluminum Alloys	Crystallographic Orientation

20. ABSTRACT (Continue on reverse side if necessary and identify by block number)

This report summarizes the results of a ~~two-phase~~ study involving: (1) experimental characterization and analytical modeling of fatigue crack tip micromechanics in aerospace structural (~~Al and Ti~~) alloys; and (2) identification and modeling ~~of~~ key factors controlling subcritical crack growth and unstable fracture in single crystal nickel-base superalloys.

(continued)

DD FORM 1473 EDITION OF 1 NOV 65 IS OBSOLETE

UNCLASSIFIED

SECURITY CLASSIFICATION OF THIS PAGE (When Data Entered)

The first section ~~of the report~~ summarizes ~~several~~ studies in which measured crack tip parameters and microstructural characterization are incorporated into a recently developed crack tip geometric model which interrelates microstructure with fatigue crack growth. The model is used with 7075-T651 Al, 7091 P/M Al, and Ti-6Al-4V to predict crack growth increments (striation spacings), which are then compared with experimental measurements for the Al alloys. Additional crack tip characterization was performed on an experimental high temperature aluminum alloy (HTAL). By using a recently developed SEM high temperature cycling stage, crack tip yielding and extension was characterized at 315°C, which showed that the interfaces of certain microstructural elements unique to the HTAL alloy were detrimental to its resistance to elevated temperature fatigue crack growth. The second section describes

In the second section of the report, the results of ambient temperature crack growth tests of single crystal Mar-M200 ~~are described.~~ Tests were carried out as functions of stress intensity range, normal stress to shear stress ratio, and crystallographic orientation, and their effect on mode of cracking and crack growth characteristics was established. Interpretation and modeling of the observed behavior are outlined.

Keywords: Crack tip plasticity; Crack growth modeling; Crystallographic orientation.

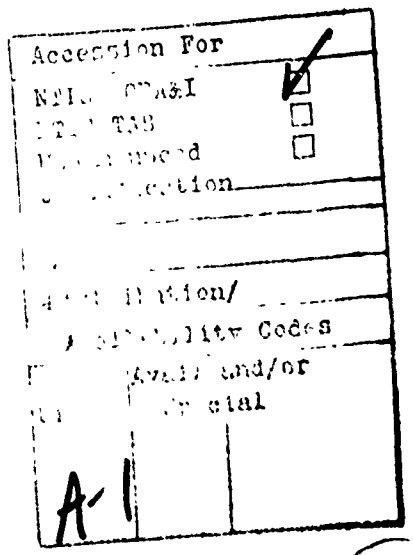

TABLE OF CONTENTS

TABLE OF CONTENTS (CONTINUED)

LIST OF TABLES

LIST OF FIGURES

LIST OF FIGURES (CONTINUED)

I. RESEARCH OBJECTIVES

A. Task 1. Influence of Metallurgical Structure Upon Crack Tip Micromechanics

1. Define experimentally the physical basis and extent of crack advance in alloys of varying, well-characterized microstructure.

2. Determine and measure experimentally the microstructural and micromechanical elements which control subcritical crack advance.

3. Incorporate microstructural and crack tip micromechanical parameters into a fundamental crack growth model.

B. Task 2. Fracture Mechanisms in Single Crystal Nickel-Base Superalloys

1. Determine the influence of crystallographic orientation on subcritical crack growth and unstable fracture.

2. Identify the relative importance of shear and normal stresses on slip band cracking.

3. Define the role of slip character on subcritical crack growth and unstable fracture.

4. Develop a model for prediction of fracture behavior.

II. STATUS OF THE RESEARCH EFFORT

A. Task 1. Influence of Metallurgical Structure Upon Crack Tip Micromechanics

1. Scope

In years past, work in the aluminum phase of this contract has focussed on measuring crack tip parameters associated with the growth of fatigue cracks. Crack tip opening displacement and mode of crack opening, crack tip strain and the distribution of strain ahead of the crack, plastic zone size, and striation spacing are all parameters which have been measured for a variety of aluminum alloys. Last year, a model was formulated which had as its purpose the consolidation of all of these factors into a coherent description of the crack growth process [1].

The geometric crack growth model [1] brings together measured crack tip opening displacements, strain, and striation spacing and observations as to how cracks actually grow, when observed under high resolution conditions. The response of the material to the applied load is assumed to be the generation of dislocations at the crack tip, with their subsequent motion along slip lines. The net displacement along these slip lines generates the observed crack opening displacement and strain.

Microstructural characteristics of the material are brought into this model through the factor which limits the length of the slip lines, and, more generally, through the cyclic flow stress. This blocked slip line concept requires a microstructural factor capable of blocking slip; therefore, it is applicable to only materials having complex microstructures, such as the high strength aluminum and titanium alloys.

This report summarizes several studies which use the combination of measured crack tip parameters, geometric model and microstructure to derive additional information about how microstructure relates to the growth of fatigue cracks. Complete crack tip and striation measurements were made on the two aluminum alloys 7075-T651 and MA-67 (now 7091); these results have already been published [2-5]. The geometric model has been used with these materials to determine the microstructural feature which limits slip line length.

Similar crack tip measurements were also made for Ti-6Al-4V, but striation spacings were not measured. In contrast to the aluminum alloys, however, the microstructure of the titanium alloy is sufficiently well understood to predict the likely length of slip lines. Thus, the model has been used with this microstructural information to predict striation spacings, which could be matched with measurements, which were subsequently made.

By way of these modeling efforts, the efficacy of the geometric model could be tested. The results of computing the striation spacings for Ti-6Al-4V were very encouraging because the predicted values were very close to those actually measured. Consequently, it is believed that the microstructural feature implicated by the model in controlling slip line length in the aluminum alloys is likely to be correct.

In the sections which follow, modeling work is summarized on these specific systems:

- o 7075-T651 dry and wet air
- o MA-87 (7091) vacuum and wet air
- o Ti-6Al-4V vacuum and wet air

In addition, fatigue crack growth was observed in an experimental aluminum alloy, HTAL, at ambient temperature and at 315°C in our high temperature cyclic loading stage for the SEM [6].

Composition, metallurgy and properties of each of these alloys are given in Table I. There are both similarities (yield strength) and differences (grain size) among the aluminum alloys studied. Microstructures of each of the alloys are shown in Figure 1. The microstructural feature showing the most similarity is the dispersoid volume fraction and size between 7075 and 7091. These factors were measured for both the alloys, and the results are given in Table II.

2. Current Status

a. Modeling Fatigue Striation Spacing for Ti-6Al-4V

Modeling of the titanium alloy is considered first because for this material the slip distance was chosen from the microstructure and the model was used to predict the resultant striation spacing. Striation spacing was then measured using both SEM and replica-TEM methods. Table III summarizes the results obtained; the agreement between prediction and measurement is considered to be excellent. Crack growth increment (striation spacing) is predicted to increase by a factor of 10 between threshold and $\Delta K = 15$ MN/m$^{3/2}$ for growth in a vacuum, while for growth in air, the increase is only a factor of 3 for the same range of ΔK.

Besides the excellent agreement between striation spacings predicted and measured, two other results lend confidence to the modeling. The model predicts, and observation confirms, that the amount of Mode II crack opening is less for this alloy than for the aluminum alloys. The model also predicts that CTOD must be defined further away from the crack tip for large values of ΔK, if the relation between crack opening displacement and distance from the tip is to be linear on a log-log plot, which is the condition found experimentally.

Table I. Composition, Metallurgy and Properties of Alloys

Alloy	7075	7091 (MA-87)	Ti-64	HTAL
Composition	Al-5.6Zn-2.5Mg-1.6Cu	Al-6.5Zn-2.5Mg-1.5Cu-0.8Co	Ti-6Al-4V	Al-8.8Fe-3.8Ce
Fabrication	Ingot cast and rolled	Air atomized, compacted, ABC-triple upset forged and extruded	Unknown	Air atomized* extruded 10:1
Heat Treatment	-T651	-T7E69	Recrystallized Annealed	Unknown
Grain Structure (length, width, thickness)	Large pancake (130x60x18 μm)	Small, elongated (5x2x2 μm)	Equiaxed (10 μm)	0.25-0.5 μm (subgrains)
Tensile Yield Strength (MPa) (0.2% strain offset)	508	503	862	360
Cyclic Stress-Strain $\Delta\sigma$ (MPa) =	$1550\ (\frac{\Delta\varepsilon_p}{2})^{.0594}$	$1548\ (\frac{\Delta\varepsilon_p}{2})^{.067}$	$2550\ (\frac{\Delta\varepsilon_p}{2})^{.15}$	Unknown

*The remainder of the processing is unknown. Alloy made by Alcoa.

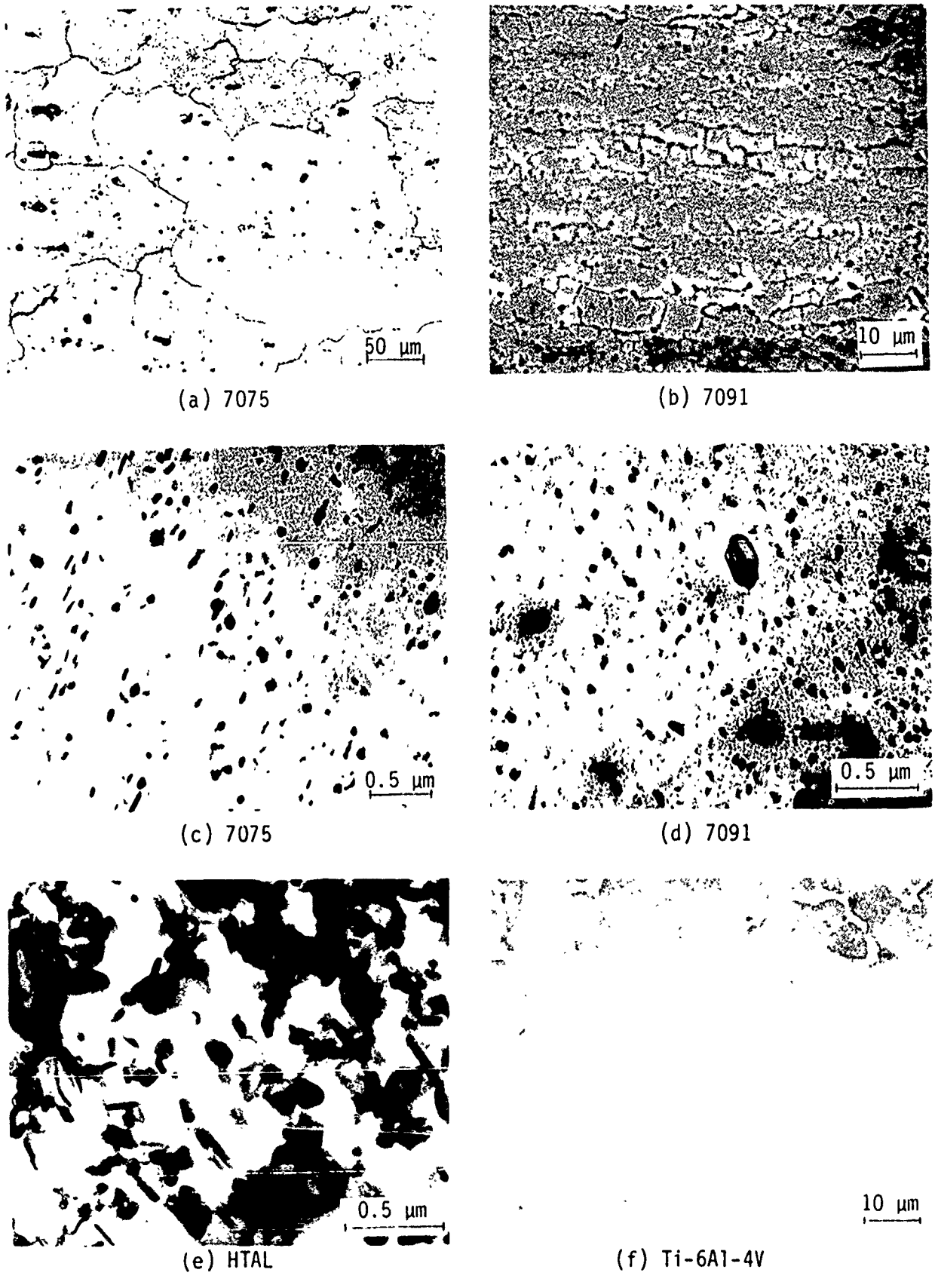

Figure 1. Microstructures studied showing the differences between 7075 and 7091 (a) and (b), but the similarities between 7075, 7091 and HTAL (c, d and e). (f) shows the titanium alloy microstructure.

Table II. Dispersoid Characterization

	7075-T651	7091-T7E69 (MA-87)	HTAL
Size range of dispersoids counted (μm)	0.02 to 0.08	0.02 to 0.1	0.06
Foil thickness (μm)	0.15 to 0.2	0.12 to 0.2	0.1
Volume fraction of dispersoids (f)	0.008 to 0.011	0.010 to 0.017	0.04
Mean free path (MFP) μm	3.7 to 5	4.6 to 7.5	1 to 2

Table III. Results of Model, Ti-6Al-4V

Ti-6Al-4V Measured Striation Spacings
$\Delta K = 8 \pm 1$ MN/m$^{3/2}$

Environment	Predicted by Model (μm)	Measured (μm)
Vacuum	0.034	0.1*
Air	0.131	0.133 ± .04

*Striations nearly impossible to find. This is the result of only one measurement and could be in considerable error.

Crack tip geometries computed using the model are shown in Figure 2. Comparison is made at both effective ΔK and applied ΔK. These results indicate that the modeling procedure is probably a reasonably correct representation of a fatigue crack tip, and that it is possible to identify an appropriate parameter in the microstructure which is limiting the length of slip lines. These results have given us much more confidence in the crack tip parameter-model-microstructure relation, and have caused us to believe that the results for aluminum alloys are credible.

b. Modeling to Determine the Microstructural-Slip Limiting Parameter in Aluminum Alloys

For the aluminum alloys 7075 and 7091, the geometric model was used to determine the length of slip lines which fit the correlation of measured CTOD, strain and striation spacing. Results are given in Table IV. These values should be compared with those in Table II, the dispersoid spacing. The agreement with dispersoid mean free path is certainly much better than with any other microstructural parameter, and as a consequence of this good correlation, it is the mean free path between dispersoids which is believed to be limiting the slip line length in these alloys. Because the dispersoid characteristics between these two alloys are so similar, the similarity in fatigue crack growth characteristics at intermediate ΔK is not surprising. There is a difference in crack growth rates for these alloys in the near-threshold region, but that is due to a change in the opening mode mix between the two alloys; the microstructural characteristic responsible for this material response has not been identified.

The crack tip geometries predicted using the model are shown in Figures 3 and 4. Comparison is made at the same effective ΔK for both alloys and environments. The shift from mainly Stage I at low ΔK to mostly Stage II should be noted, as should the much larger component of Mode II crack opening for the 7091. The larger Mode II probably is indicative of a shear instability in the 7091, which promotes larger strains at the crack tip, which in turn, allows the crack to grow more rapidly. This is especially true at ΔK values near threshold. Direct observation has shown that crack opening in Mode II can occur at a lower load than crack opening in Mode I for near-threshold ΔK. A full understanding of this phenomena has not been obtained yet, but is under study.

c. Direct Observation of Crack Growth in an Experimental High Temperature Aluminum Alloy

The newly completed high temperature SEM cyclic loading stage [6] was used to observe crack growth in an experimental Al-Fe-Ce alloy of the composition and metallurgy given in Table I, and having the microstructure shown in Figure 1(e). Fatigue cracks in this alloy were observed to lengthen in much the same way as in 7075 and 7091. The main exception to this was when the crack path came close to a "Zone A" particle. These particles are regions approximately 5 micrometers in diameter thought to have solidified much more rapidly than the other powder particles from which the alloy was made. These small particles are much harder and more deformation resistant than the matrix.

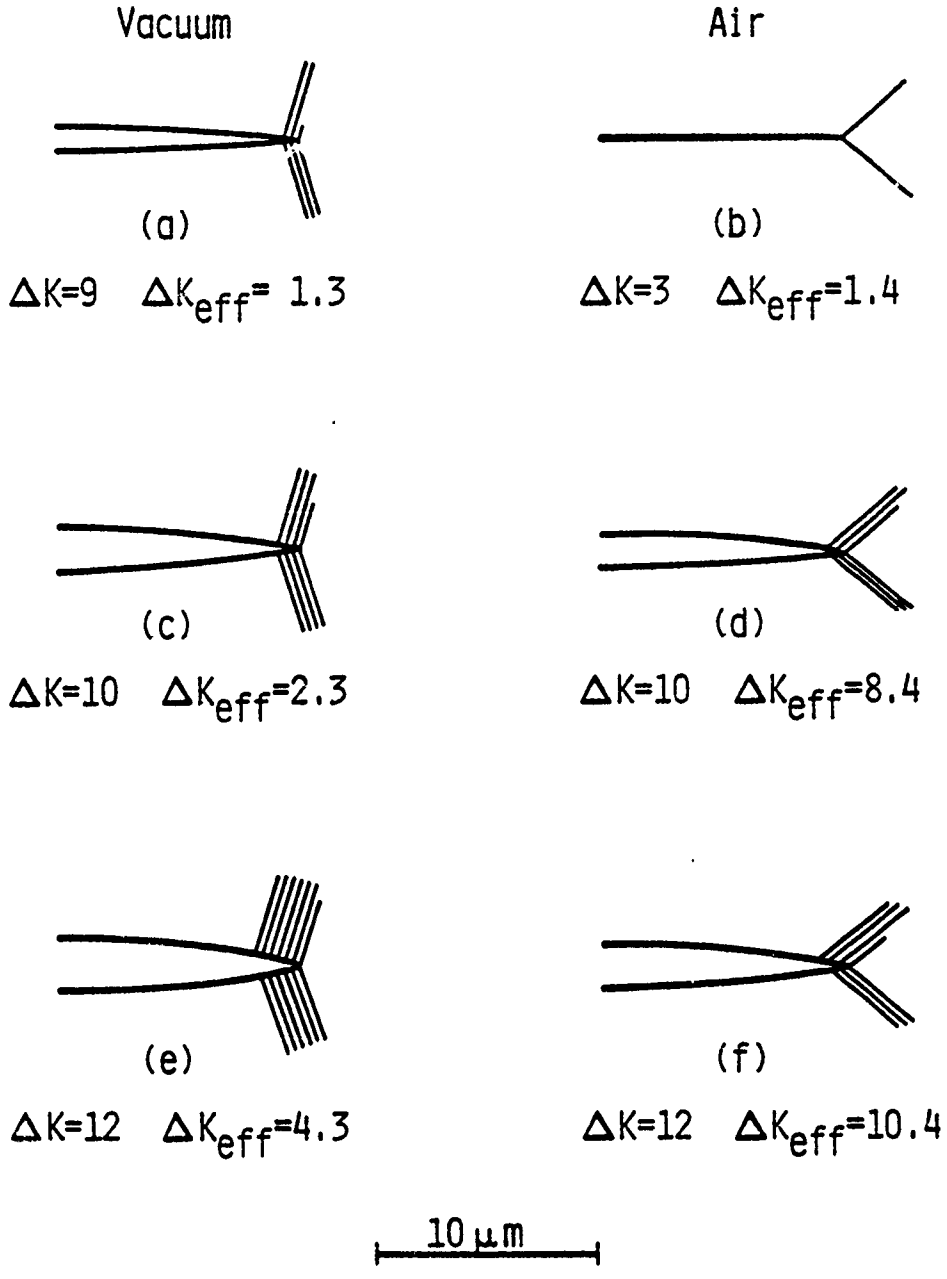

Figure 2. Ti-6Al-4V(RA). Results of the crack tip geometric model relating crack tip strain, opening displacement, microstructure and crack growth rate. Comparisons made at constant ΔK_{eff}, (a) and (b), and at constant ΔK (c-f).

Table IV. Slip Distances Derived Using the Geometric Crack Tip Model

	7075	r_s (μm)	7091
Vacuum	7.2		5.1
Air	5.0		6.9

All values ± 2 μm.

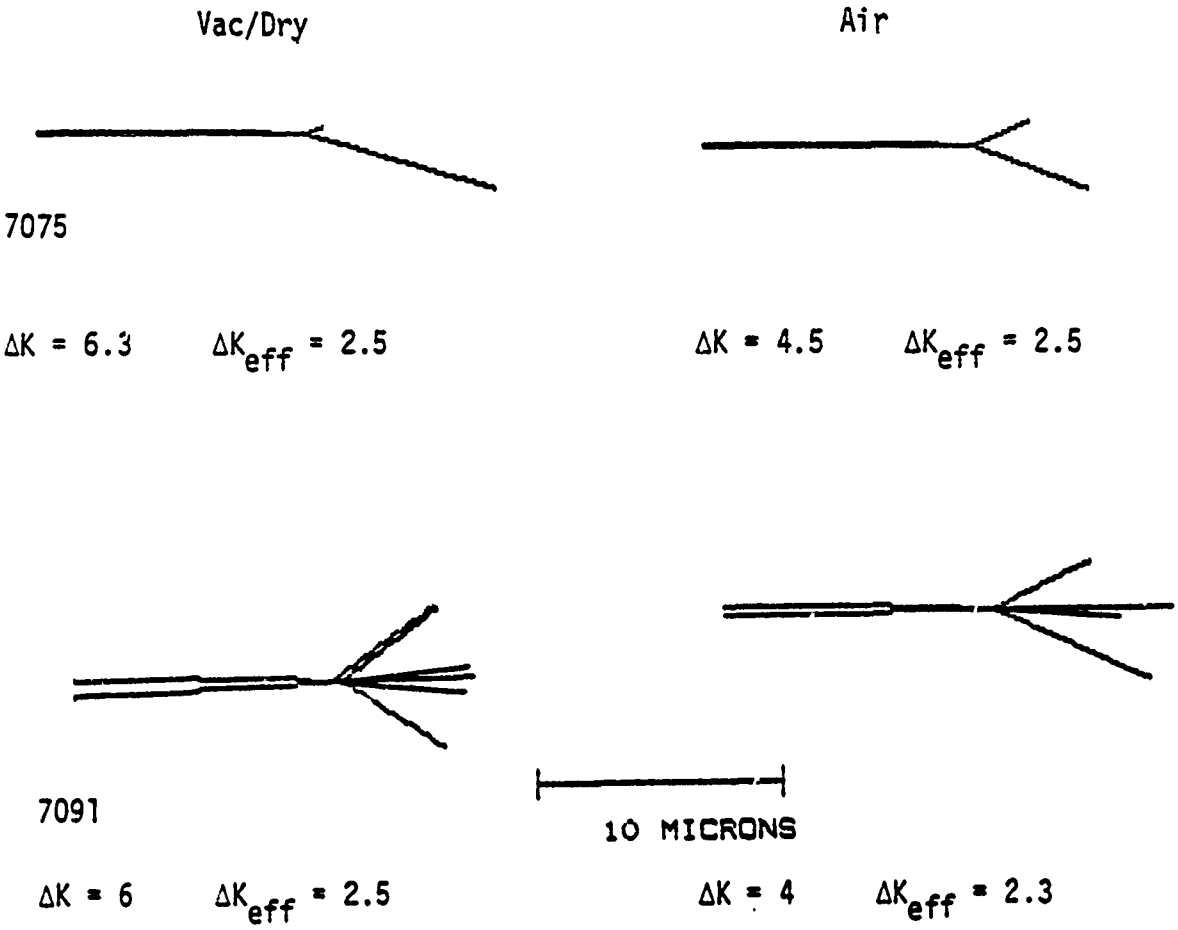

Figure 3. Crack tip-slip line geometry as determined using the geometric crack tip model. Comparison is made at equivalent low values of ΔK_{eff}.

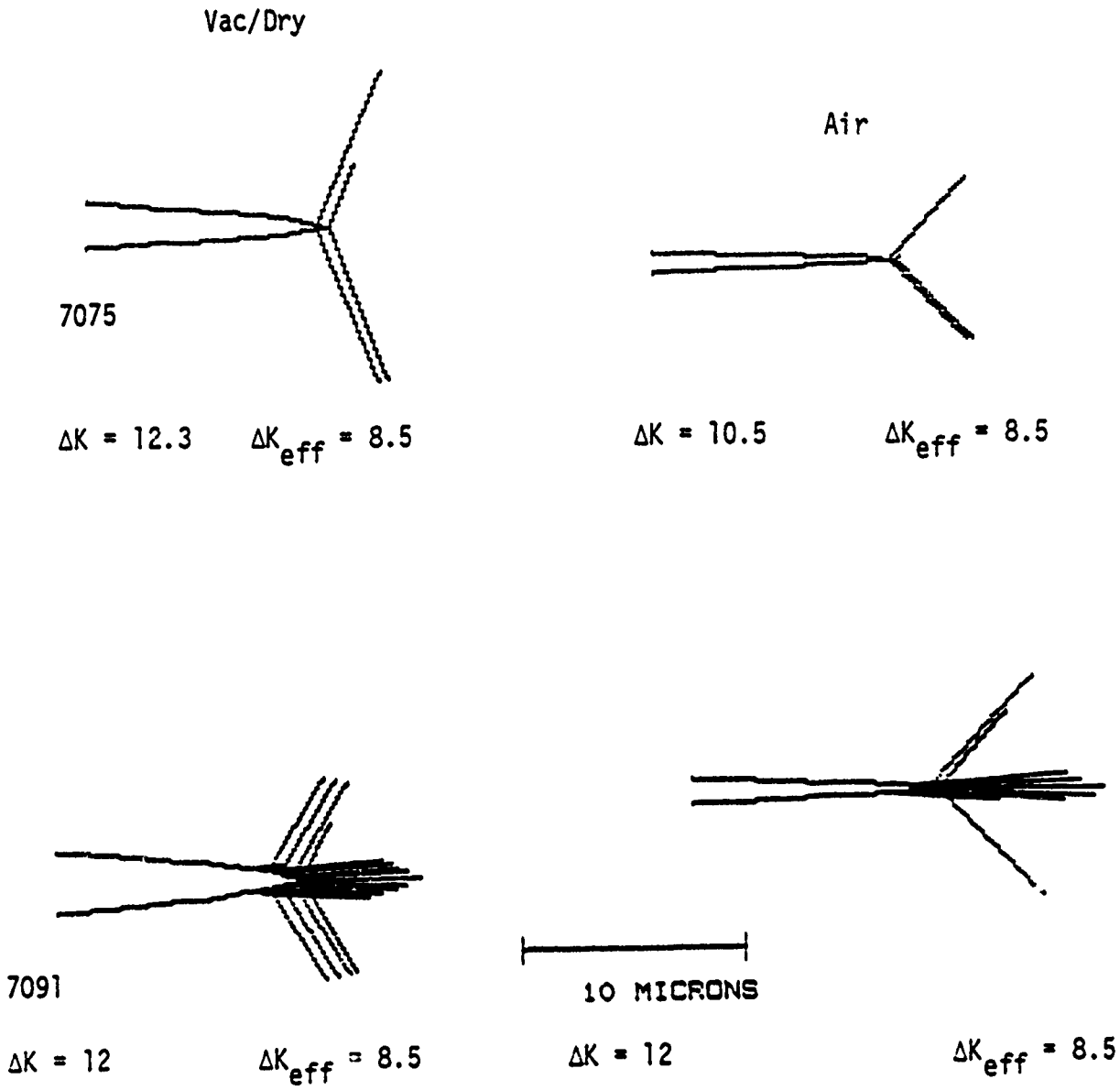

Figure 4. Crack tip-slip line geometry as determined using the geometric crack tip model. Comparison is made at equivalent higher values of ΔK_{eff}.

When a fatigue crack approaches within 5 to 10 micrometers of a "Zone A" particle, the otherwise nearly smoothly varying strain field around the crack tip is perturbed, and the crack path deviates toward the particle. A typical sequence of events is shown in Figure 5, which shows successive photographs of the crack tip region as it interacts with a "Zone A" particle. The microstructure of the matrix/particle interface is shown in the micrograph in the lower portion of the photograhic montage. The interface region seems to be lacking the dispersoid structure of either the matrix or the particle. Consequently, the interface is weaker than the particle or the matrix. This is confirmed by the fact that the crack grows through the interface region when possible. Thus, the existence of the "Zone A" particles is detrimental to fatigue crack advance in this material. Essentially, the same sequence of events shown in Figure 5 was observed at both ambient and 315°C (600°F).

In addition to the still photographs of Figure 5, a videotape was made showing a similar sequence of events, and the alloy developers at Lockheed California Company and Alcoa were shown the tape and otherwise apprised of the detrimental characteristics of "Zone A" particles.

Limited examination of this alloy by transmission electron microscopy has indicated that the average dispersoid volume fraction and size are not largely different from those found for 7075 and 7091. The volume fraction of dispersoid shown in Table II (0.05) is less than actually measured (0.16) because many of the dispersoids appear to be clumped together in masses, which, although they increase the volume fraction, do not actually increase the slip-limiting capability of the material. The volume fraction of 0.16 compares favorably with 0.22 derived from work of Fine and Weertman [7], who used different methods of measurement. The slip line distance shown in Table II is a reasonable estimate, but it is based on limited data and could be in error by a factor of at least 3. The value of 1-2 μm given in Table II is probably on the high end of the actual average mean free path.

Grain size for HTAL is similar to that for 7091, although there may be different texture effects between the two which lead to differences in misorientation between adjacent grains. Etching characteristics and TEM diffraction results lead to this conclusion. The main similarity between HTAL, 7091 and 7075 is the mean free path length and dispersoid spacing.

As a consequence of the modeling results and the microstructural similarity between these aluminum alloys, taken together with actual observations that the sequence of events attending fatigue crack growth is similar in 7075, 7091 and HTAL matrix (excluding interaction with "Zone A" particles), the general crack growth rates of these alloys should be similar, which they are, in fact, found to be. Figure 6 shows a comparison between 7091 and limited data on HTAL at both ambient and 315°C.

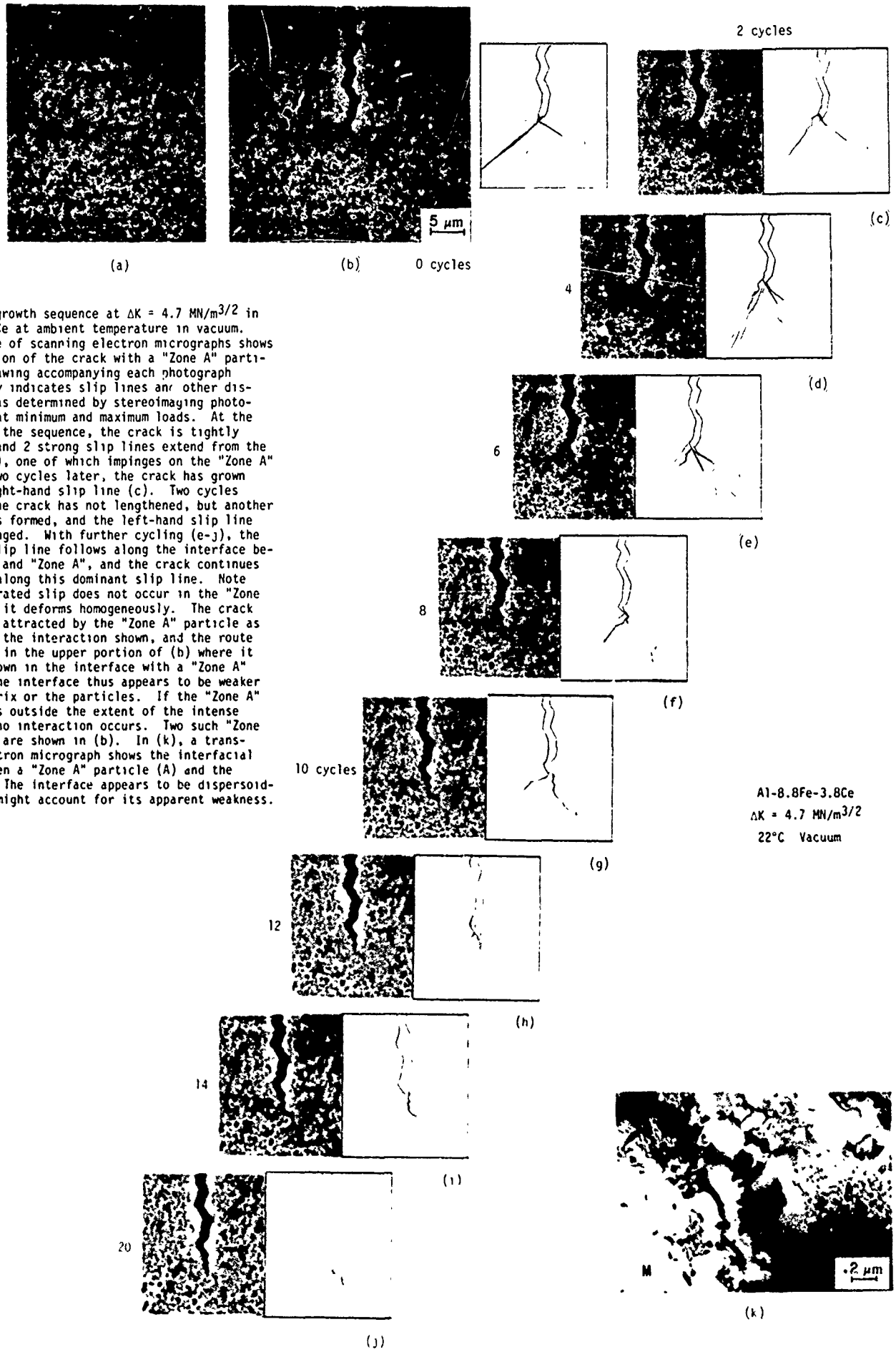

Crack growth sequence at $\Delta K = 4.7$ MN/m$^{3/2}$ in Al-8.8Fe-3.8Ce at ambient temperature in vacuum. This sequence of scanning electron micrographs shows the interaction of the crack with a "Zone A" particle. The drawing accompanying each photograph schematically indicates slip lines and other displacements, as determined by stereoimaging photographs made at minimum and maximum loads. At the beginning of the sequence, the crack is tightly closed (a), and 2 strong slip lines extend from the crack tip (b), one of which impinges on the "Zone A" particle. Two cycles later, the crack has grown along the right-hand slip line (c). Two cycles later (d), the crack has not lengthened, but another slip line has formed, and the left-hand slip line has also changed. With further cycling (e-j), the right-hand slip line follows along the interface between matrix and "Zone A", and the crack continues to lenghten along this dominant slip line. Note that concentrated slip does not occur in the "Zone A" particle; it deforms homogeneously. The crack is evidently attracted by the "Zone A" particle as evidenced by the interaction shown, and the route of the crack in the upper portion of (b) where it again has grown in the interface with a "Zone A" particle. The interface thus appears to be weaker than the matrix or the particles. If the "Zone A" particle lies outside the extent of the intense slip lines, no interaction occurs. Two such "Zone A" particles are shown in (b). In (k), a transmission electron micrograph shows the interfacial region between a "Zone A" particle (A) and the matrix (M). The interface appears to be dispersoid-free, which might account for its apparent weakness.

Figure 5. Fatigue Crack - "Zone A" - Interaction.

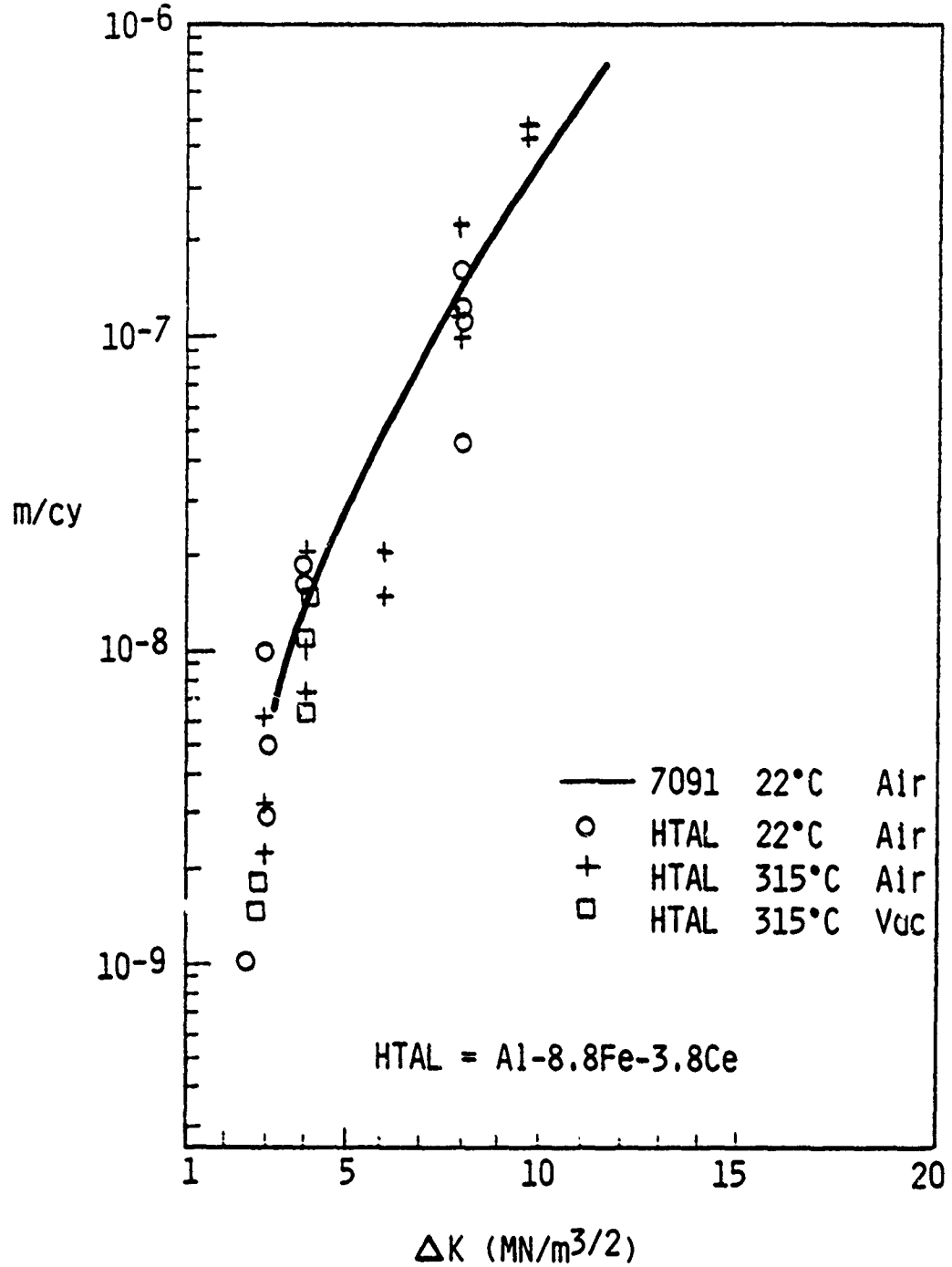

Figure 6. Measured fatigue crack growth rate of the high temperature aluminum alloy Al-8.8Fe-3.8Ce at room and 315°C as compared to 7091.

3. References

[1] D. L. Davidson, Acta Met., 32, 1984, 707.

[2] J. Lankford and D. L. Davidson, Acta Met., 31, 1983, 1273.

[3] D. L. Davidson and J. Lankford, Fat. Eng. Mat. Struct., 6, 1983, 241.

[4] D. L. Davidson and J. Lankford, Fat. Eng. Mat. Struct., 7, 1984, 29.

[5] D. L. Davidson and J. Lankford, Mat. Sci. Eng. (in press).

[6] A. Nagy, J. B. Campbell, and D. L. Davidson, Rev. Sci. Instr., 55, 1984, 778.

[7] M. E. Fine and J. R. Weertman, "Synthesis and Properties of Elevated Temperature P/M Aluminum Alloys", AFOSR Technical Report, AFOSR Contract No. 82-0005, November, 1984.

B. Task 2. Fracture Mechanisms in Single Crystal Nickel-Base Superalloys

1. Scope

Single crystal nickel-base superalloys are increasingly utilized in advanced gas turbine engine applications because of superior creep-rupture properties. In contrast to conventionally cast alloys, the mechanical properties of this class of alloys are highly anisotropic. Very little, if any, information is available on the influence of anisotropy on the mechanisms of crack growth. The current program is aimed at identifying and modeling the key factors controlling subcritical crack growth and unstable fracture in single crystal nickel-base superalloys. Using single crystal Mar-M200 as a model material, the efforts so far have been focused on two areas: (1) the influence of crystallographic orientation on subcritical crack growth and unstable fracture, and (2) the relative importance of shear and normal stresses on slip band cracking.

2. Current Status

Fatigue crack growth tests have been performed for both unidirectional and multiaxial cyclic loading, using compact-tension and tubular specimens, respectively. Crack growth rates have been determined at ambient temperature as functions of stress intensity range, the normal stress to shear stress ratio, and crystallographic orientation. The results indicate that in most cases, subcritical crack growth occurs by a coplanar slip mechanism either along a single {111} slip plane or on ridges formed with two {111} slip planes. Crack extension by an alternating slip process has also been observed, however. The effects of crystallographic orientation, stress state, and crack closure on the mode of cracking and the resulting crack growth behavior will be discussed as follows: (a) multiaxial fatigue crack growth and (b) fatigue crack growth and closure in unidirectionally-loaded Mar-M200 single crystals.

a. Multiaxial Fatigue Crack Growth

(1) Experimental Procedures

Mar-M200 single crystal tubular specimens were fatigued at room temperature in a multiaxial testing machine by applying combined cyclic axial loads and torques. The specimen geometry, test procedure, and the microstructure of the material have been reported earlier [1] and will not be repeated here. A summary of the loading conditions, tube axis, and the notch orientation for individual specimens is shown in Table I. Figures 1(a) and (b), show, respectively, the orientations of the tube axis and the notch (slot) in the cubic stereographic triangles.

Table I. A Summary Of The Cracking Mode, Fracture Plane, And The Critical Stress Intensities At Overload Fracture For Mar-M200 Single Crystals Tested At A Variety Of Stress States And Axis/Slot Orientations.

Specimens	Orientations		Applied	Cracking Modes	Fracture Planes	Critical Stress Intensities at Overload (MPa$\sqrt{m}$)			
	Axis	Slot	$\Delta\tau/\Delta\sigma$			K_{Ic}	K_{IIc}	K_{IIIc}	K^{c}_{eff}
1	[010]	[001]	.5	I, II, III	(111), ($\bar{1}$11)	29.9	25.1	21.0	50.7
2	[010]	[001]	1.0	I, II, III	(111), ($\bar{1}$11)	32.3	21.2	20.7	49.8
3	[010]	[001]	2.0	I, II, III	(111), ($\bar{1}$11)	32.6	14.0	23.0	49.1
4	[010]	[101]	.5	I, II	(111) & (1$\bar{1}$1) Ridges	66.4	16.4	-	68.4
5	[010]	[101]	1.0	I, II	(111) & (1$\bar{1}$1) Ridges	56.4	28.1	-	63.1
6	[010]	[101]	2.0	I, II	(111) & (1$\bar{1}$1) Ridges	39.5	39.5	-	55.9
7	[01$\bar{1}$]*	12° off [111]	1.0	I, II	($\bar{1}$11)	-	-	-	-
8	[01$\bar{1}$]*	10° off [011]	1.0	I, II	(111) & ($\bar{1}$11) Ridges	-	-	-	-
9	[01$\bar{1}$]	[211]	2.0	I, II	(1$\bar{1}$1) & ($\bar{1}$11)	58.1	40.9	-	71.0
10	[311]†	$\simeq$ [$\bar{1}$22]	1.0	I, II	(111) & (1$\bar{1}$1) Ridges	65.5	32.7	-	73.2

* Specimens did not fracture

† 22° off [001]

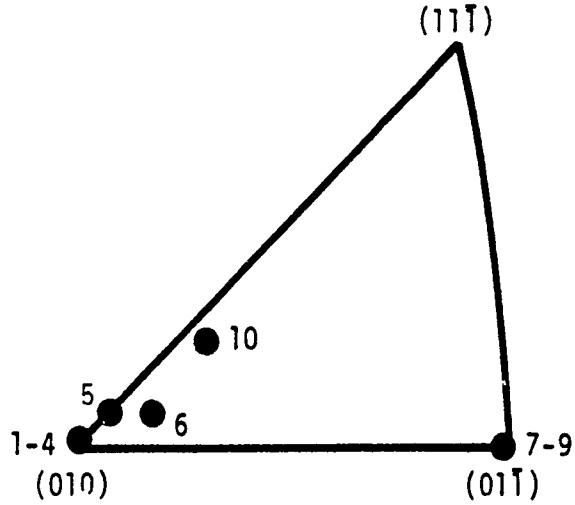

(a)

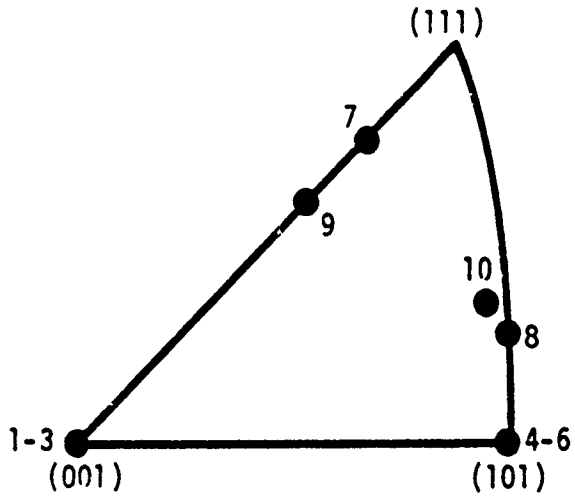

(b)

Figure 1. The orientations of the tube axis and the notch in a cubic stereographic triangle: (a) the tube axis orientation, and (b) the notch orientation.

(2) Crack Geometries, Fracture Paths and Fractographic Observations

The macroscopic fatigue crack geometries observed in modified Mar-M200 single crystals are summarized in Figure 2 together with the orientations of the tube axis and the notch (slot). Figure 2 indicates that the fatigue cracks may lie normal, inclined, or parallel to the tube axis, depending on the axis and notch orientations. In Figures 2(a) and (e), the cracks are also inclined through the thickness of the specimens. Since both tensile and torsional loads are applied, the cracking modes are Mode I and II for the through-thickness cracks [Figures 2(b), (c), and (d)] but are Mode I, II and III for cracks which are inclined through the thickness [Figures 2(a) and (e)]. The procedures for computing the stress intensity factor for these complex crack geometries are described in Reference 2. It should be noted that the effective stress intensity ranges were computed on the basis of anisotropic fracture mechanics using the idealized crack geometries shown in Figure 2. The critical stress intensity factors at which overload fracture occurred were also computed and summarized in Table I.

The crystallographic planes on which the dominant cracks propagate belong to {111}. As summarized in Table I, the fatigue crack propagation occurred on either a single {111} plane or on two equally-stressed {111} planes. In most cases, the crack was seen to follow the slip band ahead of the crack tip [Figure 3(a)]. However, non-crystallographic crack propagation by a process which appears to involve alternating slip on two slip systems was also observed [Figure 3(b)]. The characteristics of the fracture surface of Mar-M200 single crystals are: (1) a cleavage-like fracture appearance is observed in all specimens, and (2) fracture surface ridges in specimens failed on two equally-stressed {111} planes. The cleavage-like fracture surface appears to be the consequence of cracking along a single coplanar slip plane [3,4], while the ridges are formed as the result of simultaneous slip and cracking on two equally-stressed cross-slip planes which are both coplanar with the crack. Both these mechanisms are dictated by the crack-tip stress field, and are directly related to the slip process occurring at the crack tip.

(3) Stress State Effects on Crack Propagation Rate

Crack growth in Mar-M200 single crystals with the [010] axis and [101] slot orientation occurred on fracture planes which were macroscopically coplanar with the notch (slot) and normal to the [010] axis [see Figure 2(b)]. The mode of cracking was typically mixed Mode I and II, and it remained unaltered when the $\Delta\tau/\Delta\sigma$ ratio was increased from .5 to 2. The crack growth rates are plotted as a function of the applied ΔK_I, ΔK_{II}, and ΔK_{eff} in Figures 4(a), (b), and (c), respectively. From Figures 4a and b, it is clear that the crack growth rate

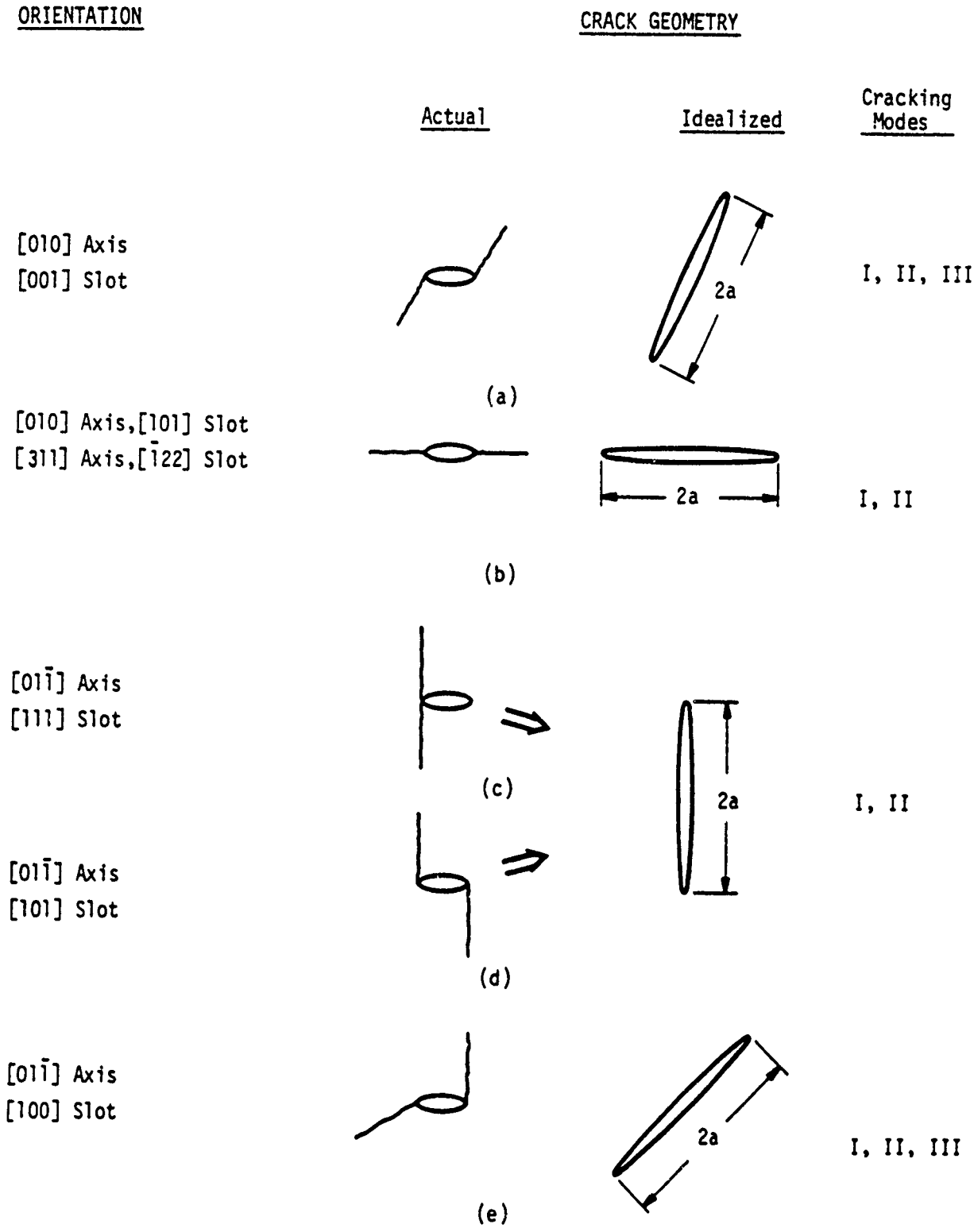

Figure 2. A summary of the crack geometries observed in Mar-M200 single crystals and their idealizations used in computing the stress intensity factors.

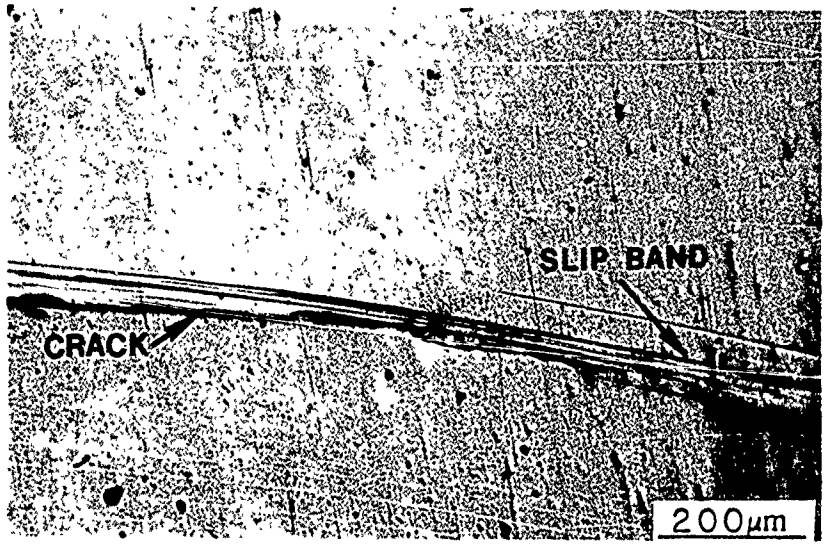

(a)

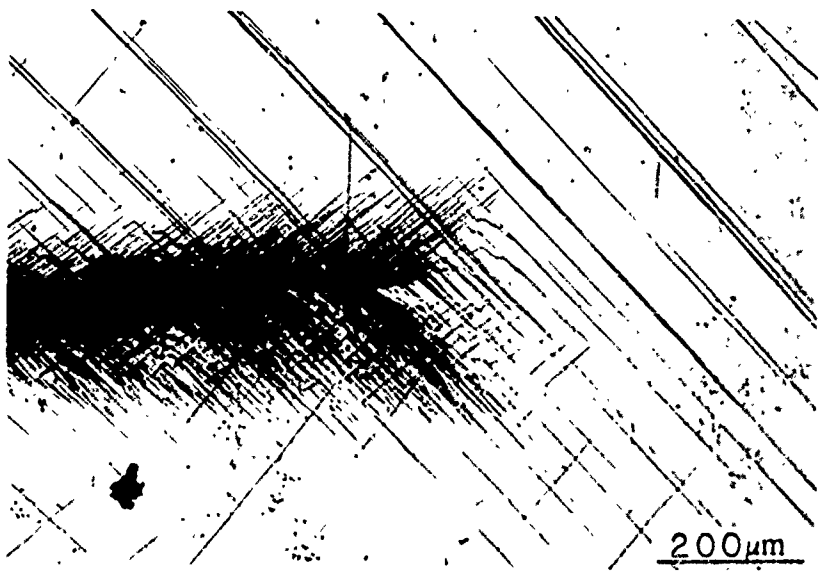

(b)

Figure 3. Crack-tip slip morphology in Mar-M200 single crystals: (a) coplanar slip is observed in all specimens, and (b) 45° slip bands are observed in the [010] axis/[101] notch and the [311] axis/[$\bar{1}$22] notch specimens at high ΔK_{eff} and at one of the two crack tips only.

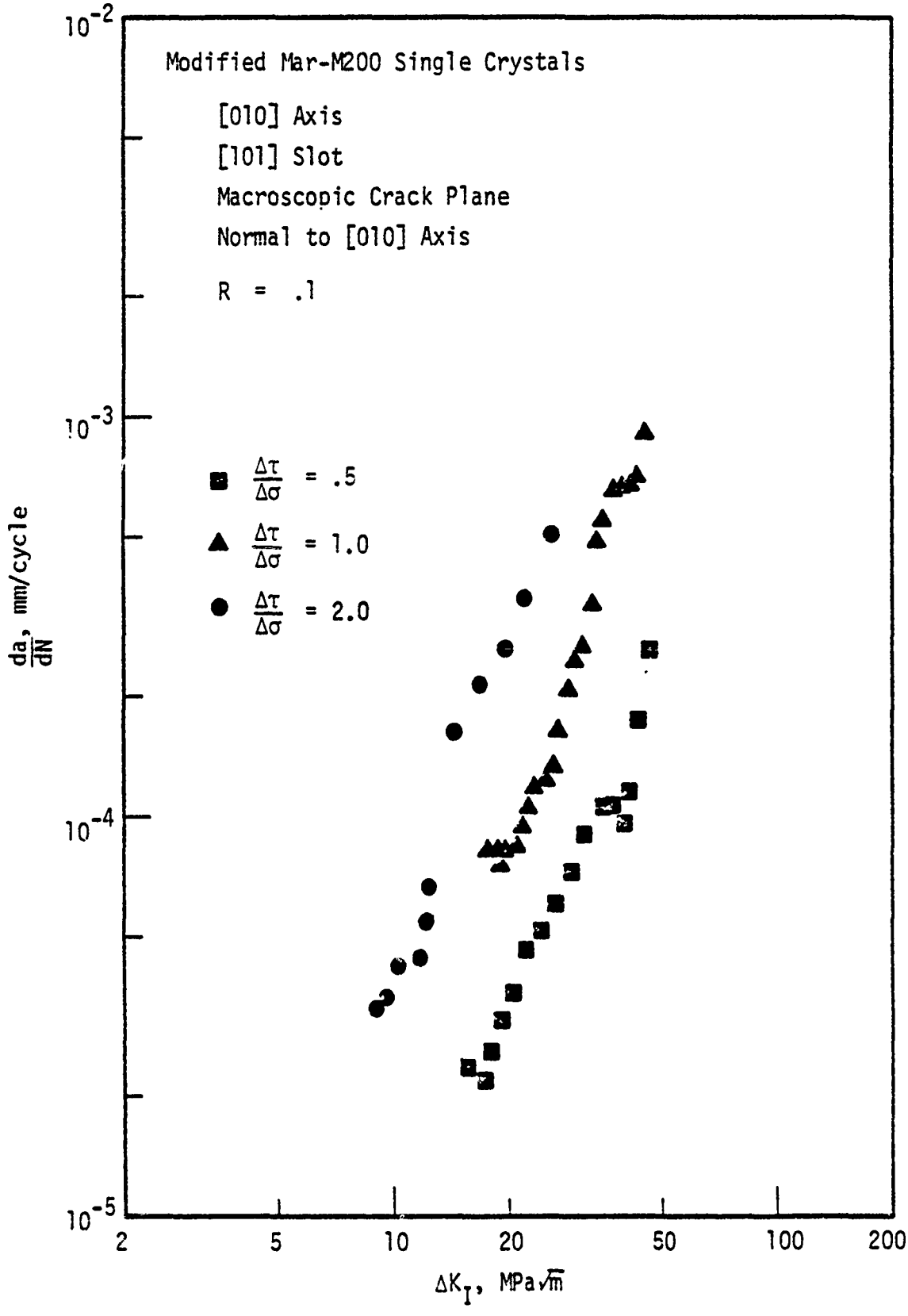

4(a)

Figure 4. The crack growth rates of the [010] axis/[101] slot specimens fatigued at $\Delta\tau/\Delta\sigma$ ratios of .5, 1, and 2 are plotted as a function of: (a) the Mode I stress intensity range, (b) the Mode II stress intensity range, and (c) the effective stress intensity range.

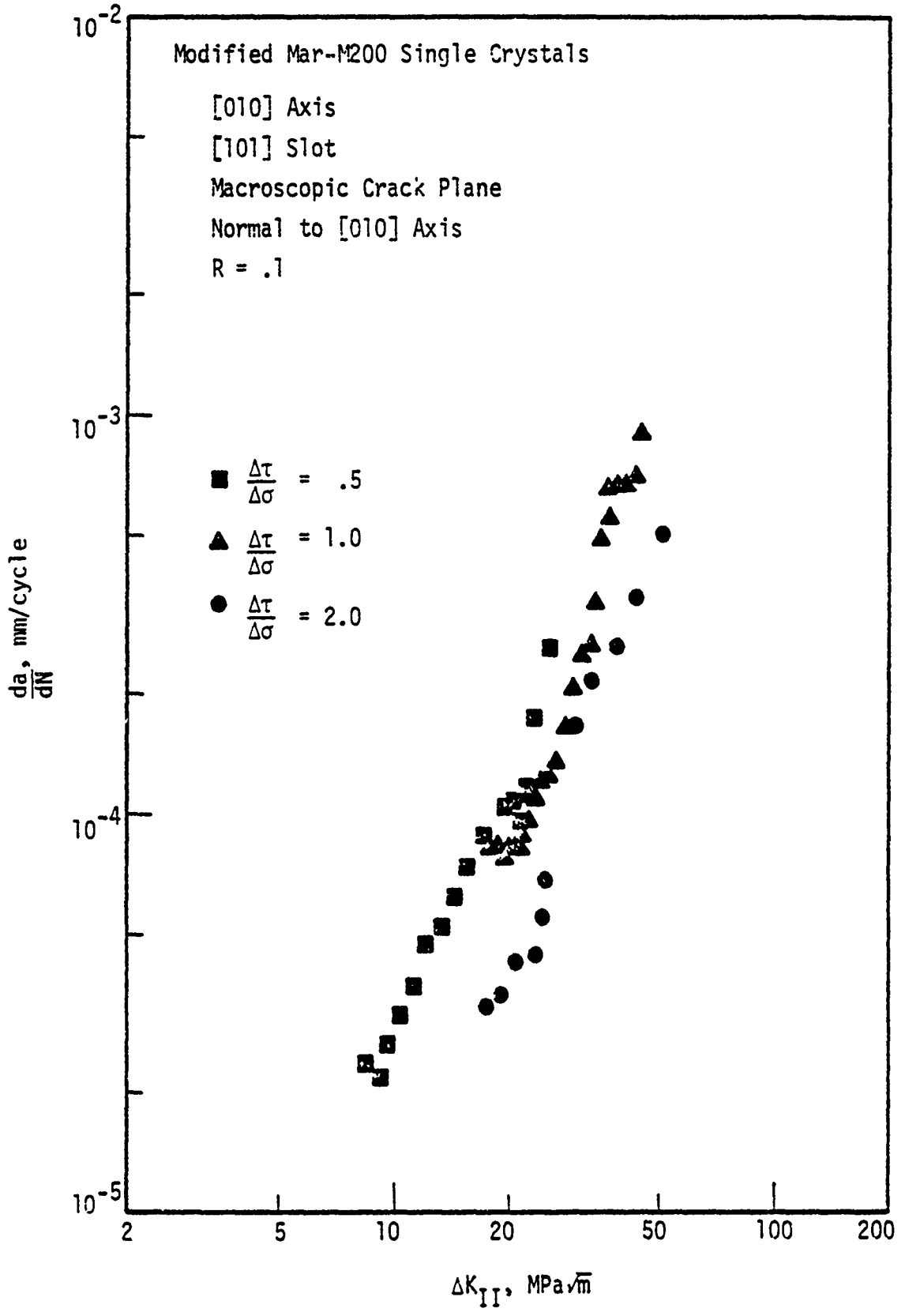

4(b)

Figure 4. The crack growth rates of the [010] axis/[101] slot specimens fatigued at $\Delta\tau/\Delta\sigma$ ratios of .5, 1, and 2 are plotted as a function of: (a) the Mode I stress intensity range, (b) the Mode II stress intensity range, and (c) the effective stress intensity range.

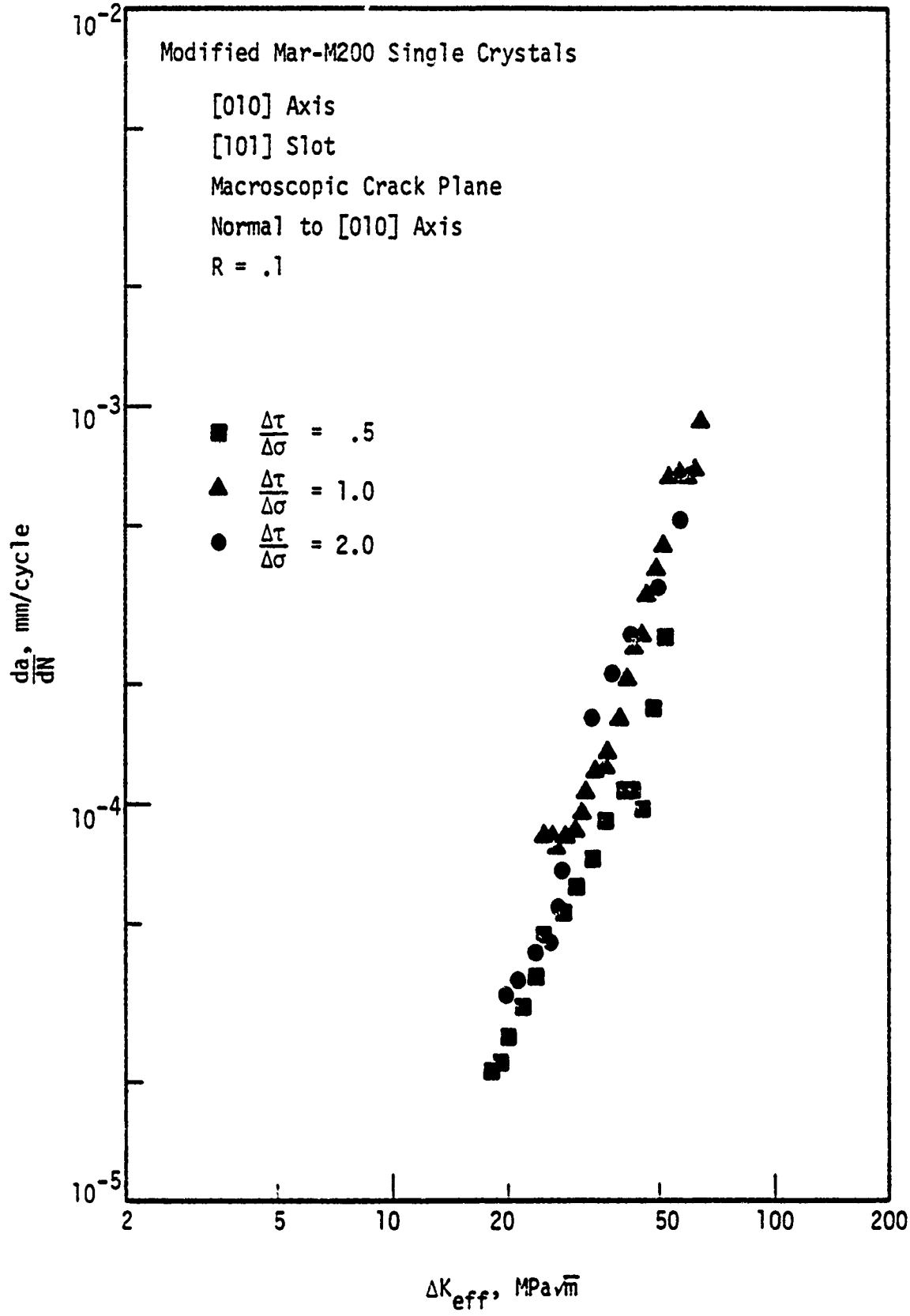

4(c)

Figure 4. The crack growth rates of the [010] axis/[101] slot specimens fatigued at $\Delta\tau/\Delta\sigma$ ratios of .5, 1, and 2 are plotted as a function of: (a) the Mode I stress intensity range, (b) the Mode II stress intensity range, and (c) the effective stress intensity range.

data for the various $\Delta\tau/\Delta\sigma$ ratios cannot be correlated with either ΔK_I and ΔK_{II} alone. On the other hand, the same set of data forms one small scatter band when plotted as a function of ΔK_{eff} in Figure 4(c). The potential ramification of this result is that ΔK_{eff} might be the driving force for multiaxial fatigue crack growth and the crack growth rate, uniquely defined by the ΔK_{eff} parameter, would then be independent of the applied $\Delta\tau/\Delta\sigma$ ratio.

A unique relationship between the crack growth rate and ΔK_{eff}, however, is not observed in Mar-M200 single crystals with the [010] axis/[001] slot orientation. Fatigue crack advance in these specimens was mixed Mode I, II, and III with the left and right cracks propagating on two different {111} planes [(111) and ($\bar{1}$11)] which were inclined through the thickness of the specimens. Plotted as a function of ΔK_{eff} in Figure 5a, the crack growth rates showed a strong dependence on the applied stress state (the $\Delta\tau/\Delta\sigma$ ratio). In particular, the crack growth rate at a given ΔK_{eff} increased as the $\Delta\tau/\Delta\sigma$ ratio decreased, indicating that crack propagation was more rapid under tensile stresses than under shear stresses. The stress state effect appears to be the manifestation of crack closure in which the fracture surfaces make contact prior to the attainment of the minimum loads or torques. Analyses indicate that the normal stress acting on the crack plane is compressive during part of the loading cycle. The presence of such a compressive stress would cause crack closure and reduce the $\Delta\tau$ range at which the crack remains open, thereby reducing the driving force for crack growth and the crack propagation rate [5]. The normal stress range ($\Delta\sigma_{op}$) and the shear stress range ($\Delta\tau_{op}$) at which the crack remains open have been calculated to be .8, .7, and .62 for the $\Delta\tau/\Delta\sigma$ values of .5, 1, and 2, respectively. Using these stress values for recomputing the effective stress intensity range, the dependence of the crack growth rate on the $\Delta\tau/\Delta\sigma$ ratio is reduced, though not completely eliminated, as shown in Figure 5(b).

(4) Effects of Crystallographic Orientation

Once the effects of stress state and crack closure have been established, the influence of crystallographic orientation on multiaxial fatigue crack growth in Mar-M200 single crystals can be examined. Figure 6 compares the crack growth data for the single crystal specimens of various axis/notch orientations tested at $\Delta\tau/\Delta\sigma$. As indicated earlier, the [010] axis/[001] notch specimens are affected by crack closure; the effective ΔK for these specimens are therefore based on $\Delta\sigma_{op}$ and $\Delta\tau_{op}$. A significant observation of Figure 6 is that the fatigue crack growth rate is at most mildly dependent on the influence of crystallographic orientation. Considering the vastly different fractographic features exhibited in these specimens, the orientation-insensitive crack growth behavior is surprising. However, it can be rationalized on the basis of similitude as most, if not all, of the fatigue crack growth in

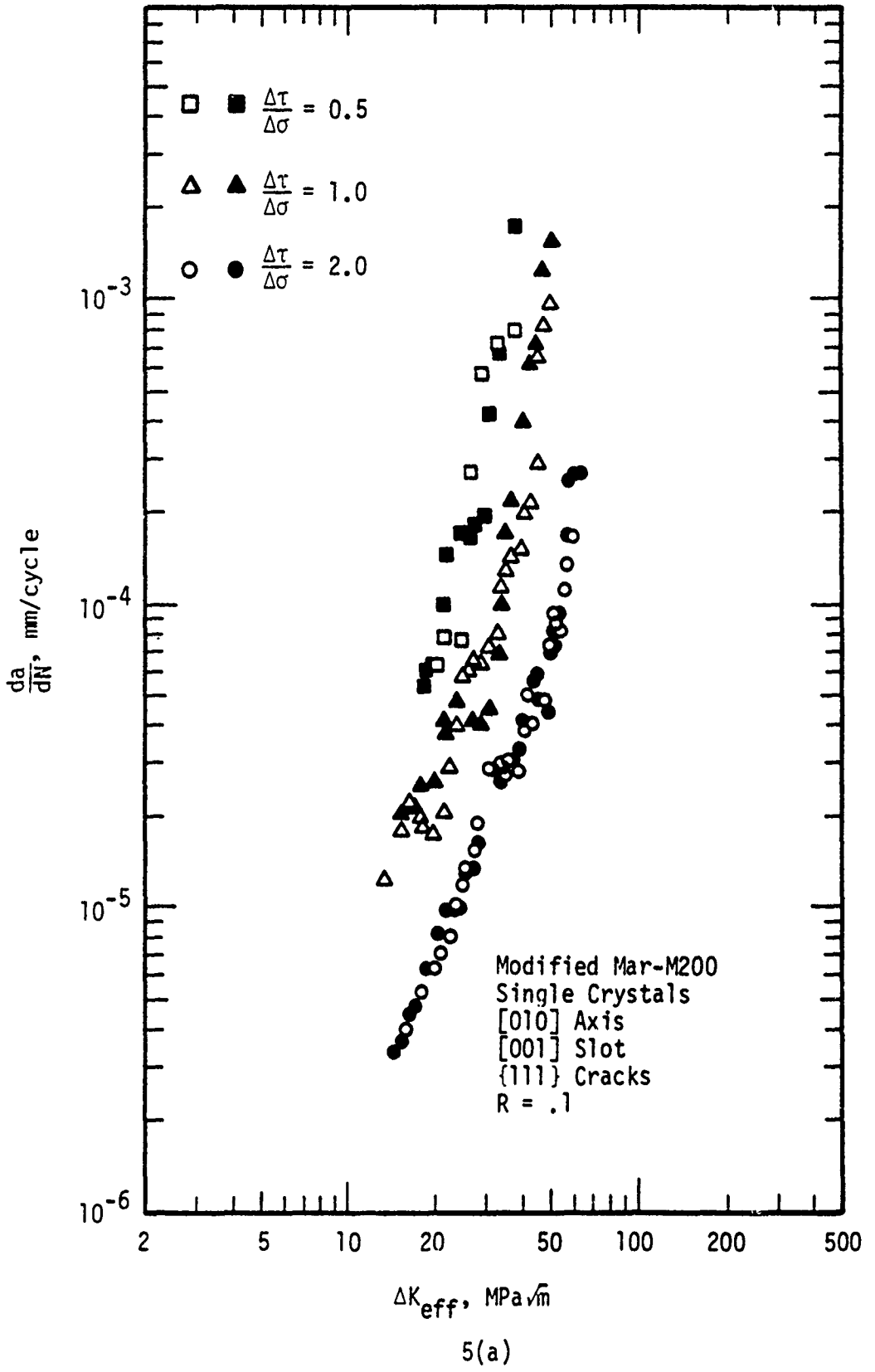

Figure 5. The crack growth rates of the [010] axis/[001] slot specimens fatigued at $\Delta\tau/\Delta\sigma$ ratios of .5, 1, and 2: (a) plotted as a function of the effective stress intensity range, ΔK_{eff}, and (b) plotted as a function of the effective stress intensity range, $\Delta K'_{eff}$, which is based on the $\Delta\sigma$ and $\Delta\tau$ at which the crack is not closed.

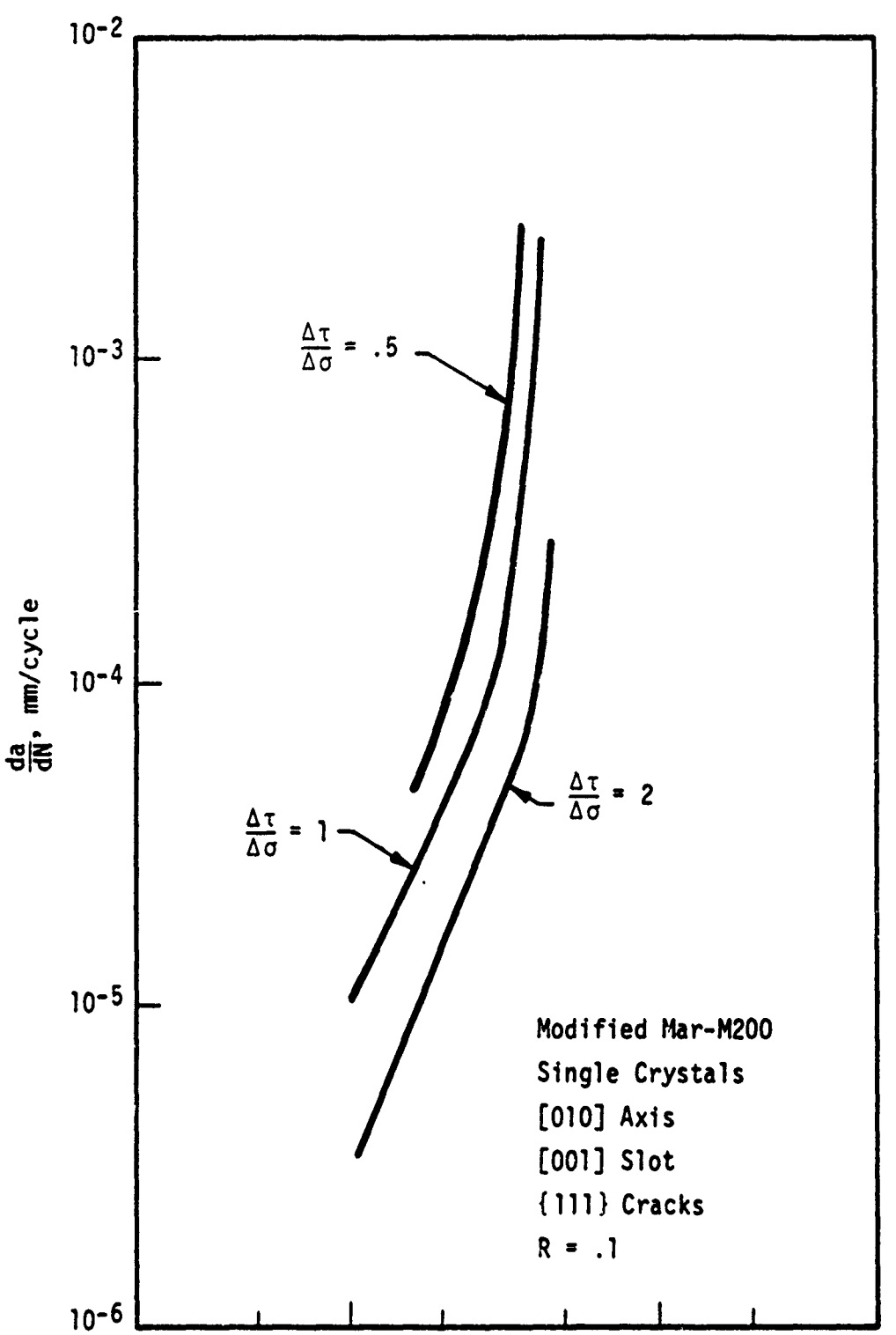

5(b)

Figure 5. The crack growth rates of the [010] axis/[001] slot specimens fatigued at $\Delta\tau/\Delta\sigma$ ratios of .5, 1, and 2: (a) plotted as a function of the effective stress intensity range, ΔK_{eff}, and (b) plotted as a function of the effective stress intensity range, $\Delta K'_{eff}$, which is based on the $\Delta\sigma$ and $\Delta\tau$ at which the crack is not closed.

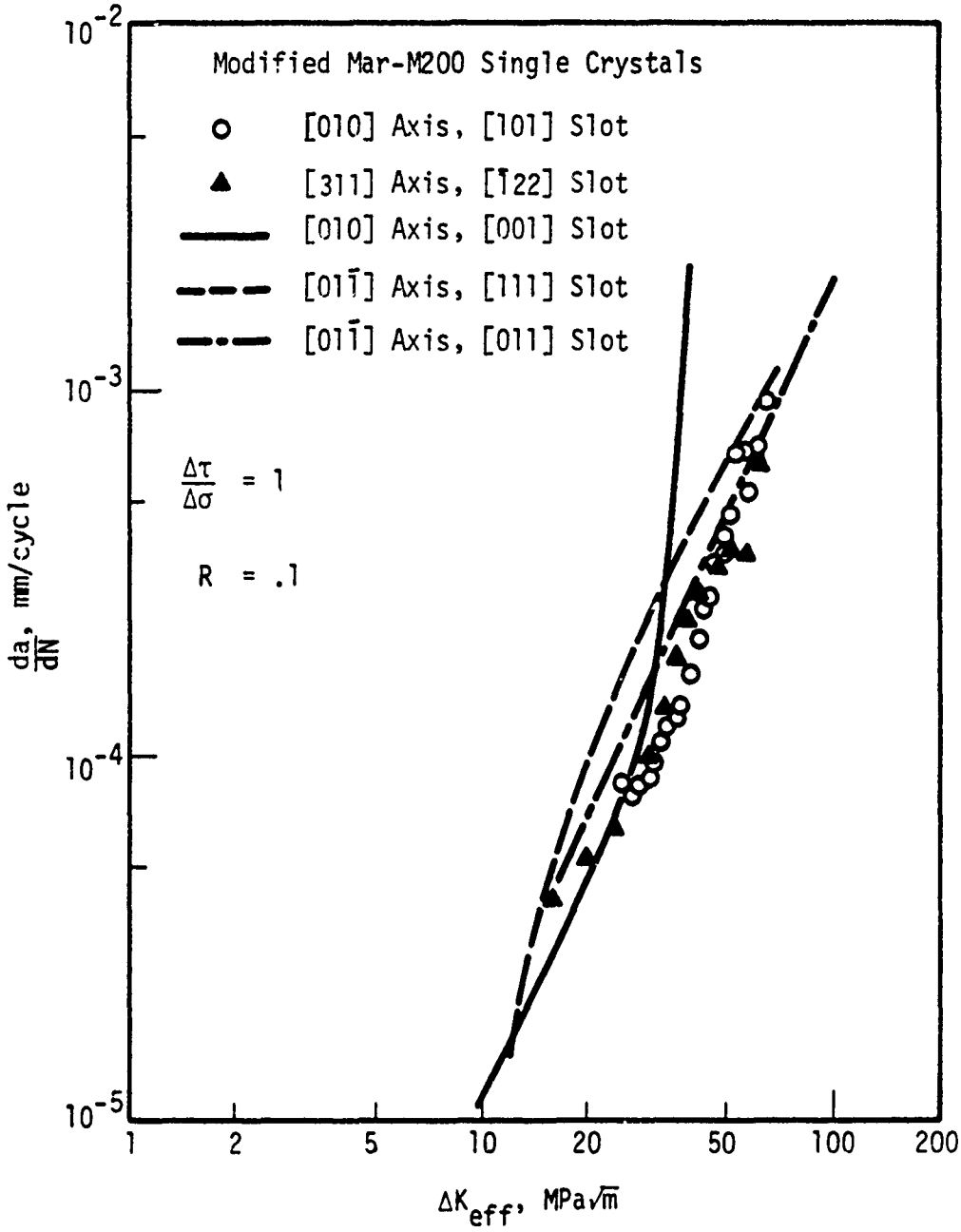

Figure 6. Comparisons of the crack growth rates of Mar-M200 single crystals at various axis and notch orientations.

the Mar-M200 single crystals occur along coplanar slip bands on either a single {111} plane or simultaneously on two cross-slip {111} planes. It is thus logical that they show comparable crack growth behavior.

(5) Discussion

One of the significant findings of the present study is that for a given axis/notch orientation, the fracture planes in extended Stage I crack growth were not altered by increasing the ratio of normal stress to the shear stress. Specifically, the [010] axis/[001] notch specimens all failed on the same two {111} planes (with the left and the right cracks propagating on a single but different {111} plane) as the $\Delta\tau/\Delta\sigma$ ratio was increased from 0.5 to 2 (Table I) and no transition from Stage I to Stage II occurred. This suggests that the classical notion of the transition of Stage I to Stage II crack growth as the normal stress becomes dominant is not applicable for this type of single crystal material.

Efforts for modeling the crystallographic crack growth process using anisotropic fracture mechanics have been initiated. By approximating the EDM notch as a crack and resolving the crack-tip stress field on all twelve {111} slip systems, the analysis reveals that, except in the cases involving cracking with fracture surface ridge formation, the fatigue cracks initiated on the planes of maximum shear stress. For the specimen orientations and loading investigated, the predicted crack planes do not vary with the applied $\Delta\tau/\Delta\sigma$ ratio, as observed experimentally.

The finding that the fatigue cracks tend to propagate along the {111} slip plane can be understood on the basis of the analysis of Koss and Chan [3,4] which examines the crack-tip stress state associated with crack propagation along coplanar slip bands. One of the key results of the analysis is the recognition that coplanar slip relaxes the shear stress components of the crack-tip field but has no effect on the normal stress components because neither the coplanar slip nor the relaxation of the crack-tip shear stresses produce displacements which are normal to the crack plane, a necessary condition for relaxing stresses which act normal to the crack plane. Dictated by the crack-tip elastic singularity, the normal stress components continue to increase up to very close to the crack tip and can be relaxed by non-coplanar slip only. Extending the Koss and Chan analysis, the current modeling efforts reveal that the coplanar slip band is generally also the plane of maximum shear stress. The presence of these large normal and shear stresses on the slip bands would explain these two observations: (1) the tendency of the fatigue crack to continue propagating along the {111} plane, and (2) the cleavage-like fracture appearance associated with coplanar slip band cracking.

The formation of fracture surface ridges can be understood in terms of simultaneous slip and cracking on two equally-stressed cross-slip planes. Figure 7 schematically demonstrates that in the [010] axis/[101] notch specimens, ridge formation can occur by simultaneous slip and cracking on the (111) and (1$\bar{1}$1) planes in the [10$\bar{1}$] direction. In a similar manner, ridges can be formed in the [01$\bar{1}$] axis/[011] notch specimen by simultaneous slip and cracking on the ($\bar{1}$11) and (111) planes in the [011] direction. In both cases, the crack growth directions coincide with the slip directions. By restricting crack growth to the slip direction, the extension of the Koss and Chan analysis indicates that large buildup of normal stress can exist ahead of a fatigue crack propagating by simultaneous slip and cracking on two equally-stressed cross-slip planes which are both coplanar with the crack; the resulting elastic-plastic crack-tip stress field is similar to that associated with fracture along a single coplanar slip band. The similitude in the crack-tip stress field suggests that there might be no significant difference between fatigue cracking along a single slip plane or on two cross-slip planes as long as they are coplanar with the crack.

b. Subcritical Crack Growth and Closure in Unidirectionally-Loaded Mar-M200 Single Crystals

Fatigue crack growth in unidirectionally-loaded Mar-M200 single crystals were studied by testing compact-tension specimens at ambient temperature at a R ratio of 0.1. The specimen geometry and experimental procedures have been reported earlier [1]. The orientations of the loading axis for individual specimens are summarized in Figure 8, as well as in Table II. The crack propagation mechanism in the unidirectionally-loaded specimens is similar to that observed under multiaxial cyclic loads. As summarized in Table II, crack growth occurred on either a single {111} plane or on two equally-stressed {111} planes which result in fracture surface ridges.

Figure 9(a) shows a typical compact-tension specimen failed by extended crystallographic cracking along a {111} plane. It should be noted that the crystallographic cracks are usually mixed-mode with Mode I, II, and III components as the cracks are inclined to loading axis and through the specimen thickness. Since there are no published results, efforts have been made to calculate the stress intensity factors for these complex crack geometries. This has been accomplished by using a computer program, dubbed BIE/CRX [6], which performs stress intensity calculations based on the boundary integral technique. These stress intensity calculations [7] were used for analyzing both the crack growth data and the critical stress intensities at which unstable fracture occurred (Table II).

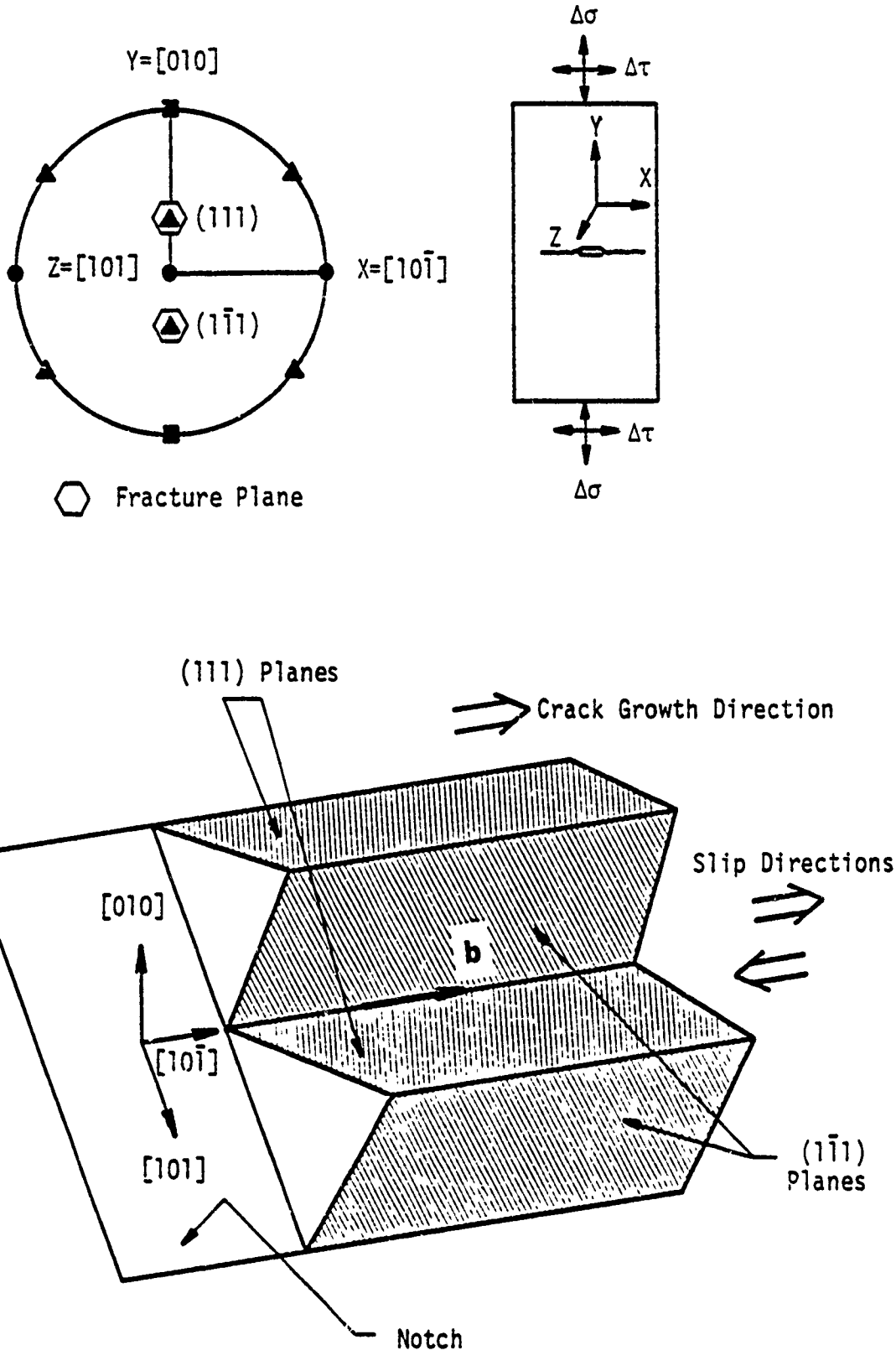

Figure 7. A schematic showing the formation of fracture surface ridges by simultaneous slip and cracking on the (1$\bar{1}$1) and (111) slip planes.

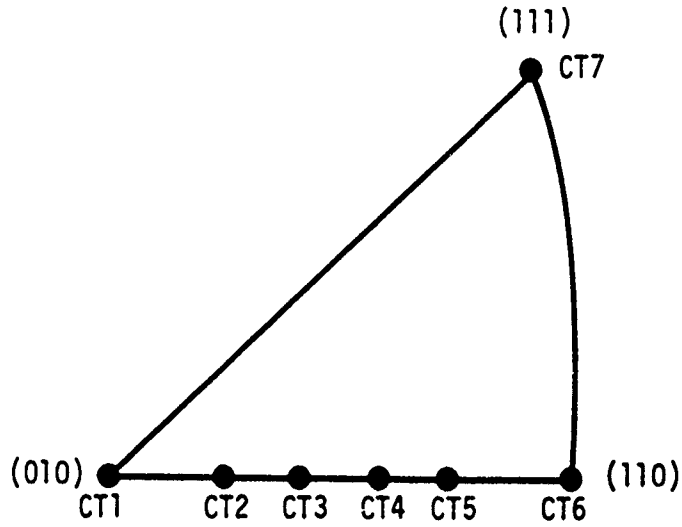

Figure 8. The orientations of the loading axis for individual Mar-M200 single crystal compact-tension specimens.

Table II. A Summary Of The Orientation Of The Stress Axis, Fracture Plane, And The Critical Stress Intensities At Overload Fracture For Mar-M200 Single Crystals Tested Under Unidirectionally Applied Cyclic Loads.

Specimen	Orientation of Stress Axis	Fracture Planes	Critical Stress Intensities at Overload ($MPa\sqrt{m}$)			
			K_{Ic}	K_{IIc}	K_{IIIc}	K^{c}_{eff}
CT1	[010]	(111) & Ridges	28.0	1.6	28.0	49.3
CT2	[150]	(1$\bar{1}$1) & Ridges	41.4	2.9	26.9	57.0
CT3	[130]	($\bar{1}$1)	55.5	3.4	32.0	72.4
CT4	[120]	($\bar{1}$11) & (1$\bar{1}$1) Ridges	34.3	$\approx$0	34.3	60.4
CT5	[230]	($\bar{1}$11) & (1$\bar{1}$1) Ridges	58.0	$\approx$0	$\approx$0	58.0
CT6	[110]	($\bar{1}$1) & Ridges	36.0	2.5	29.2	55.6
CT7	[111]	(11$\bar{1}$) & Ridges	27.6	$\approx$0	32.9	55.1

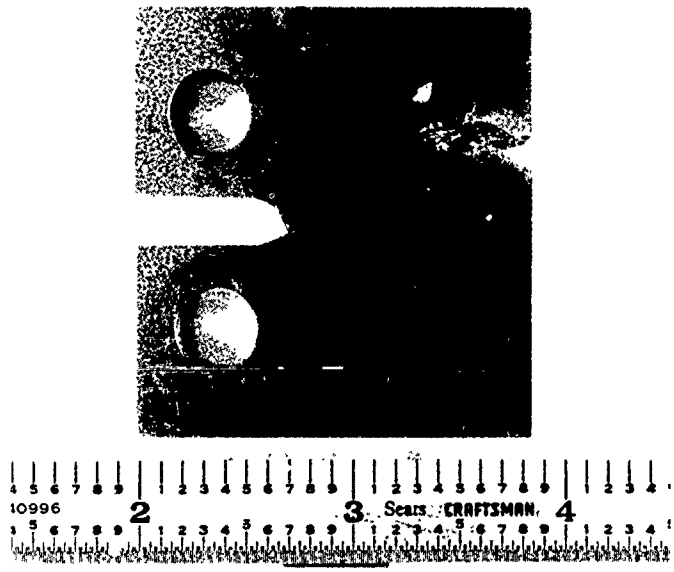

9(a)

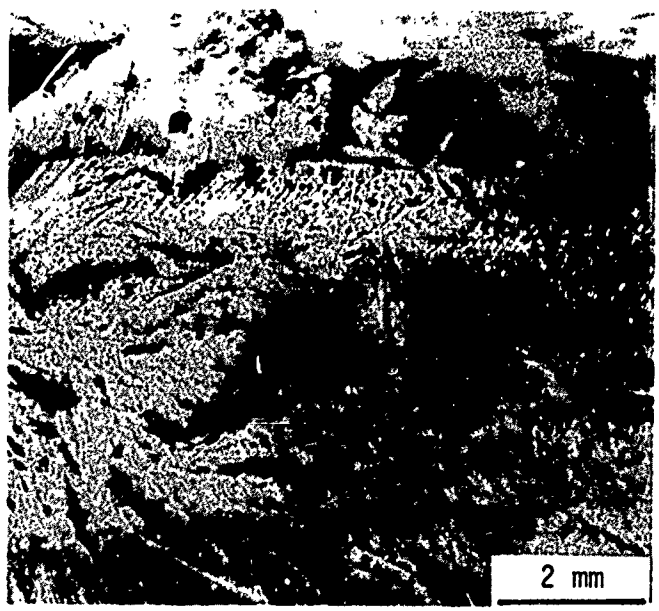

9(b)

Figure 9. Mar-M200 single crystals typically failed by extended crystallographic cracking along a {111} plane: (a) failed specimen, and (b) black debris which is believed to be oxides resulting from fretting of the fracture surface.

Figures 10 compares the crack growth rate as a function of ΔK_{eff} for specimens loaded in the [010], [110], and [111] directions, respectively. The preliminary results indicate that the [010] and [110] specimens show comparable crack growth behavior while the [111] specimen manifests slightly slower crack rate. However, it should also be pointed out that fretting-induced crack closure is a factor in these specimens. This is evidenced in Figure 9(b) which shows the presence of black debris on the fracture surface, which is believed to be oxides resulting from fretting. The presence of fretting-induced closure can reduce the stress intensity range at which the crack remains open, thereby reducing the driving force for crack growth [8]. Efforts are currently underway to assess and model the amount of fretting-induced crack closure in these specimens.

3. References

[1] J. Lankford, D. L. Davidson, G. R. Leverant, and J. E. Hack, Study of the Influence of Metallurgical Factors on Fatigue and Fracture of Aerospace Structural Materials, AFOSR Annual Report, Southwest Research Institute, 1984.

[2] K. S. Chan, J. E. Hack, and G. R. Leverant, submitted to Metallurgical Transactions, 1985.

[3] D. A. Koss and K. S. Chan, Acta Metallurgica, 28, 1245 (1980).

[4] D. A. Koss and K. S. Chan, Dislocation Modeling of Physical Systems, Pergamon Press, 1981, p. 18.

[5] W. Elber, Damage Tolerance in Aircraft Structures, ASTM STP 486, ASTM, Philadelphia, 1971, p. 280.

[6] T. A. Cruse, Applied Mathematical Modeling, 2, 287 (1978).

[7] K. S. Chan and T. A. Cruse, manuscript in preparation, 1985.

[8] S. Suresh and R. O. Ritchie, Metallurgical Transactions A, 13A, 1627 (1982).

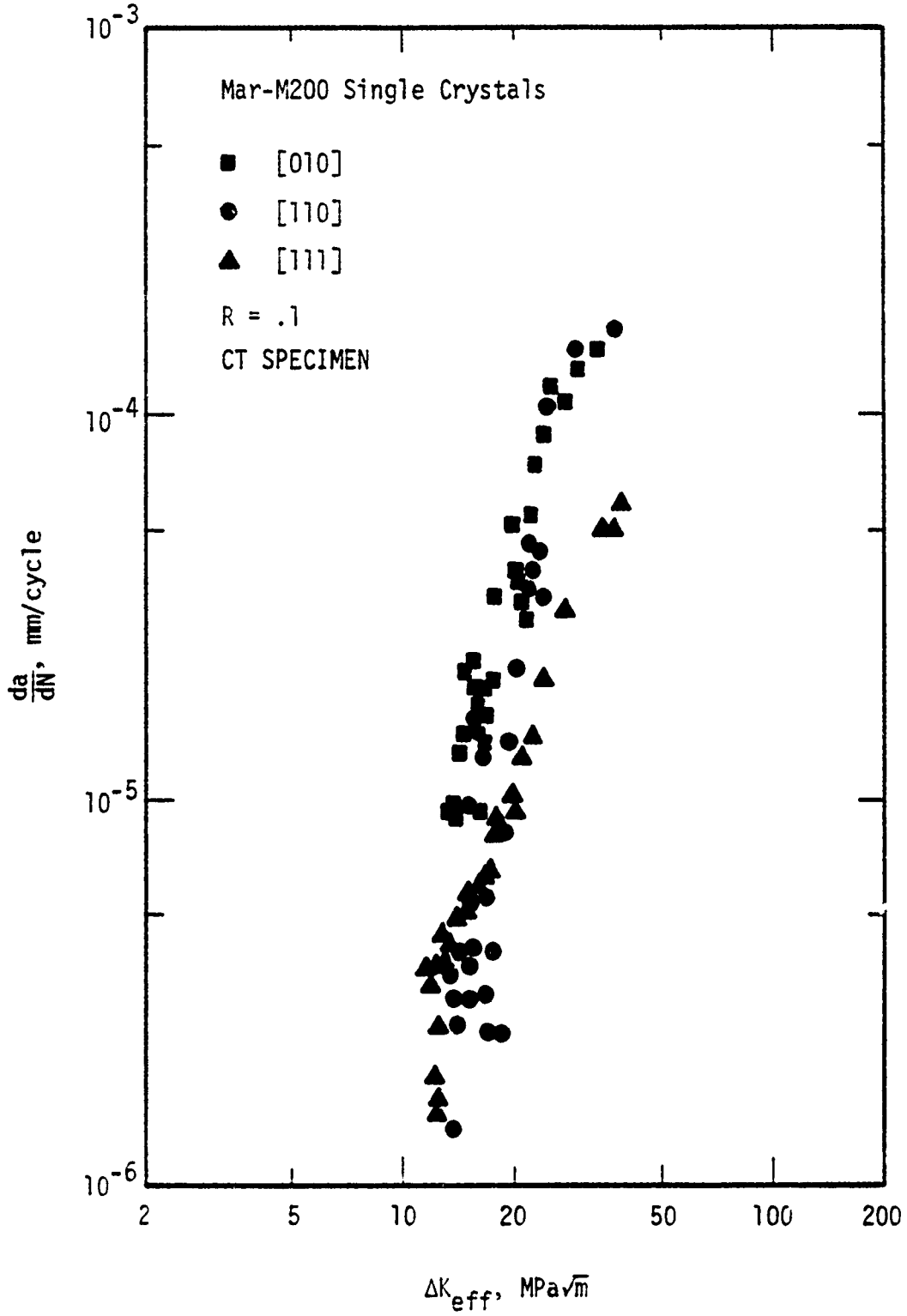

Figure 10. A comparison of the crack growth rates for the [010], [110], and [111] specimens.

III. PUBLICATIONS (AFOSR SPONSORSHIP)

A. Task 1. Influence of Metallurgical Structure Upon Crack Tip Micromechanics

1. "Experimental Mechanics of Fatigue Crack Growth: The Effect of Crack Size", D. L. Davidson and J. Lankford, Proceedings Eshelby Memorial Symposium, Cambridge University Press (in press).

2. "Experimental Mechanics and Modeling of Fatigue Crack Growth", D. L. Davidson, Proceedings of Modelling Problems in Crack Tip Mechanics, Martinus Nijhoff Publishers BV, 217, 1984.

3. "A Model for Fatigue Crack Advance Based on Crack Tip Metallurgical and Mechanics Parameters", D. L. Davidson, Acta Metallurgica, 32, 707, 1984.

4. "Fatigue CRack Growth Mechanics of Ti-6Al-4V in Vacuum and Humid Air", D. L. Davidson and J. Lankford, Metallurgical Transactions, 15A, 1931, 1984.

5. "Experimental Characterization of Fatigue Crack Tip Processes", J. Lankford and G. R. Leverant, Proceedings of the Eighth Inter-American Conference on Materials Technology, 7-7, 1984.

6. "The Effects of Aluminum Alloy Microstructure on Fatigue Crack Growth", D. L. Davidson and J. Lankford, Materials Science and Engineering (in press).

B. Task 2. Fracture Mechanisms in Single Crystal Nickel-Base Superalloys

1. "Fatigue Crack Propagation in Ni-Based Superalloy Single Crystals Under Multiaxial Cyclic Loads", K. S. Chan, J. E. Hack, and G. R. Leverant, submitted to Metallurgical Transactions, Feb. 1985.

2. "The Stress Intensity Factors for Anisotropic Compact-Tension Specimens with Inclined Cracks", K. S. Chan and T. A. Cruse, manuscript in preparation, March 1985.

3. "Fatigue Crack Growth and Closure in Unidirectionally-Loaded Mar-M200 Single Crystals", K. S. Chan, J. E. Hack, and G. R. Leverant, manuscript in preparation, March 1985.

IV. PROGRAM PERSONNEL

Name	Title	
Dr. James Lankford	Staff Scientist	Co-Principal Investigators
Dr. David L. Davidson	Institute Scientist	
Dr. Gerald R. Leverant	Assistant Director, Materials Sciences	
Mr. John E. Hack*	Senior Research Metallurgist	
Dr. K. S. Chan	Research Engineer	
Mr. Ronald McInnis	Senior Technician	
Mr. John Campbell	Senior Technician	
Mr. Harold Saldana	Senior Technician	

*Presently at Los Alamos National Laboratory.

V. INTERACTIONS - 1984

A. Task 1. Influence of Metallurgical Structure Upon Crack Tip Micromechanics

1. Videotape and montage of still photographs to Dr. Sharon Langenbeck of Lockheed (Burbank, California) and other results of work on Al-Fe-Ce high temperature aluminum alloys. Dr. Langenbeck shared these results with Dr. Greg Hildeman of Alcoa, developer of the alloy. 10 February 1984.

2. Symposium and paper - Eshelby Memorial Symposium, Sheffield, UK, on "Fundamentals of Deformation and Fracture". Paper and presentation "Experimental Mechanics of Fatigue Crack Growth: The Effect of Crack Size" by D. L. Davidson and J. Lankford. 3 April 1984.

3. Seminar - Rolls Royce Ltd., Derby, UK, "Fatigue Crack Growth in Aluminum and Titanium Alloys". 11 April 1984.

4. Dr. Norman Fleck of Cambridge University, but starting post-doctoral work at Harvard with Hutchinson and Rice, visits SwRI to discuss work on crack closure. 22 and 23 October 1984.

5. Prof. S. Suresh of Brown University visits SwRI to discuss work on crack closure, thresholds and small cracks. 23 October 1984.

B. Task 2. Fracture Mechanisms in Single Crystal Nickel-Base Superalloys

1. A paper entitled, "Fatigue Crack Propagation in Ni-Based Superalloy Single Crystals Under Multiaxial Cyclic Loads", by K. S. Chan, J. E. Hack, and G. R. Leverant, was presented at AIME 1984 Fall Meeting in Detroit, MI. 17-21 September 1984.